nature microbiology

ARTICLES

https://doi.org/10.1038/s41564-018-0167-x

Calcium sequestration by fungal melanin inhibits calcium–calmodulin signalling to prevent LC3-associated phagocytosis

Irene Kyrmizi[1,2], Helena Ferreira[3,4,18], Agostinho Carvalho[4,5,18], Julio Alberto Landero Figueroa[6], Pavlos Zarmpas[7], Cristina Cunha[4,5], Tonia Akoumianaki[1], Kostas Stylianou[1], George S. Deepe Jr[8], George Samonis[1], João F. Lacerda[9,10], António Campos Jr[11], Dimitrios P. Kontoyiannis[12], Nikolaos Mihalopoulos[7], Kyung J. Kwon-Chung[13], Jamel El-Benna[14,15], Isabel Valsecchi[16], Anne Beauvais[16], Axel A. Brakhage[17], Nuno M. Neves[3,4], Jean-Paul Latge[16] and Georgios Chamilos[1,2]*

LC3-associated phagocytosis (LAP) is a non-canonical autophagy pathway regulated by Rubicon, with an emerging role in immune homeostasis and antifungal host defence. *Aspergillus* cell wall melanin protects conidia (spores) from killing by phagocytes and promotes pathogenicity through blocking nicotinamide adenine dinucleotide phosphate (NADPH) oxidase-dependent activation of LAP. However, the signalling regulating LAP upstream of Rubicon and the mechanism of melanin-induced inhibition of this pathway remain incompletely understood. Herein, we identify a Ca^{2+} signalling pathway that depends on intracellular Ca^{2+} sources from endoplasmic reticulum, endoplasmic reticulum–phagosome communication, Ca^{2+} release from phagosome lumen and calmodulin (CaM) recruitment, as a master regulator of Rubicon, the phagocyte NADPH oxidase NOX2 and other molecular components of LAP. Furthermore, we provide genetic evidence for the physiological importance of Ca^{2+}–CaM signalling in aspergillosis. Finally, we demonstrate that Ca^{2+} sequestration by *Aspergillus* melanin inside the phagosome abrogates activation of Ca^{2+}–CaM signalling to inhibit LAP. These findings reveal the important role of Ca^{2+}–CaM signalling in antifungal immunity and identify an immunological function of Ca^{2+} binding by melanin pigments with broad physiological implications beyond fungal disease pathogenesis.

LAP is a specialized autophagy pathway linking activation of certain pattern recognition receptors (PRRs) with phagosome biogenesis[1]. LAP is a non-canonical autophagy pathway that requires assembly and activation of a unique UVRAG (UV radiation resistance associated)-containing Beclin-1–VPS34 class III PI(3)K complex for sustained PtdIns(3)P production, NOX2 complex stabilization, reactive oxygen species (ROS) release and subsequent conjugation of lipidated LC3 II on the phagosome[2]. Rubicon is a central regulator of LAP that associates with UVRAG-containing Beclin-1–VPS34 class III PI(3)K complex on the phagosome and inhibits canonical autophagy by preventing Atg14L-containing Beclin-1–VPS34 class III PI(3)K complex formation[2]. However, the signalling pathways implicated in $LC3^+$ phagosome (LAPosome) formation upstream of Rubicon and NADPH oxidase complex activation are incompletely understood.

LAP regulates diverse physiological responses and has a prominent anti-inflammatory function under steady-state conditions[3–5]. In addition, LAP has a pivotal role in host defence against the major human fungal pathogen *Aspergillus fumigatus*[2,6–9]. Specifically, activation of LAP during intracellular swelling of *A. fumigatus* conidia promotes phagolysosomal fusion and fungal killing by monocytes/macrophages[2,6–9]. Given the importance of LAP in immunity and host defence, this pathway represents a potential target during host-pathogen interactions. Recently, we reported that *Aspergillus* cell wall melanin selectively inhibits LAPosome formation to promote pathogenicity and revealed that LAP blockade is a general property of melanin pigments[7]. Intriguingly, melanin disrupts NADPH oxidase assembly on the phagosome to inhibit LAP[7]. However, the precise molecular target of melanin is currently unknown.

[1]Department of Medicine, University of Crete, Heraklion, Crete, Greece. [2]Institute of Molecular Biology and Biotechnology, Foundation for Research and Technology, Heraklion, Crete, Greece. [3]3B's Research Group - Biomaterials, Biodegradables and Biomimetics, Guimarães, Portugal. [4]ICVS/3B's - PT Government Associate Laboratory, Braga/Guimarães, Portugal. [5]Life and Health Sciences Research Institute (ICVS), School of Medicine, University of Minho, Campus de Gualtar, Braga, Portugal. [6]Department of Chemistry, University of Cincinnati/Agilent Technologies Metallomics Center of the Americas, University of Cincinnati, Cincinnati, OH, USA. [7]Department of Chemistry, University of Crete, Heraklion, Crete, Greece. [8]Division of Infectious Diseases, College of Medicine, University of Cincinnati, Cincinnati, OH, USA. [9]Instituto de Medicina Molecular, Faculdade de Medicina de Lisboa, Lisbon, Portugal. [10]Serviço de Hematologia e Transplantação de Medula, Hospital de Santa Maria, Lisbon, Portugal. [11]Serviço de Transplantação de Medula Óssea (STMO), Instituto Português de Oncologia do Porto, Porto, Portugal. [12]Department of Infectious Diseases, The University of Texas, MD Anderson Cancer Center, Austin, TX, USA. [13]Molecular Microbiology Section, Laboratory of Clinical Immunology and Microbiology, National Institute of Allergy and Infectious Diseases (NIAID), National Institutes of Health (NIH), Bethesda, MD, USA. [14]INSERM-U1149, CNRS-ERL8252, Centre de Recherche sur l'Inflammation, Paris, France. [15]Université Paris Diderot, Sorbonne Paris Cité, Laboratoire d'Excellence Inflamex, DHU FIRE, Faculté de Médecine, Site Xavier Bichat, Paris, France. [16]Unité des Aspergillus, Institut Pasteur, Paris, France. [17]Department of Molecular and Applied Microbiology, Leibniz-Institute for Natural Product Research and Infection Biology (HKI) and Friedrich Schiller University, Jena, Germany. [18]These authors contributed equally: Helena Ferreira, Agostinho Carvalho. *e-mail: hamilos@imbb.forth.gr

Because Ca^{2+} is an essential second messenger for signalling and intracellular trafficking events[10], we assessed the role of Ca^{2+} signalling in LAPosome formation and explored whether melanin interferes with activation of this pathway. Herein, we identify a Ca^{2+}–CaM signalling that depends on intracellular Ca^{2+} sources from endoplasmic reticulum, endoplasmic reticulum–phagosome association and Ca^{2+} release from the phagosome lumen, which regulates Rubicon recruitment for sustained PtdIns(3)P production, NADPH oxidase assembly and LAPosome formation. Furthermore, we provide genetic evidence on the physiological importance of Ca^{2+}–CaM in development of invasive aspergillosis. Finally, we demonstrate that Ca^{2+} sequestration by *Aspergillus* melanin abrogates peri-phagosomal Ca^{2+} release and CaM recruitment to inhibit LAP. Our studies identify an important role of Ca^{2+}–CaM signalling in antifungal immunity and assign an immunological function of Ca^{2+} binding by melanins with essential role in pathogenesis of human fungal diseases.

Results

Ca^{2+}–CaM signalling regulates *Aspergillus* LAP. Since Ca^{2+} and CaM are key regulators of general autophagy[11], it was essential to look at their role in LAP, which has not been investigated yet. Immunofluorescence staining of primary human monocytes at different time points of infection with conidia of melanin-competent (wild type (WT)) or melanin-deficient (Δ*pksP*) *A. fumigatus* revealed early, transient and selective CaM localization exclusively in the phagosomes of melanin-deficient *A. fumigatus* conidia (Fig. 1a,b). In addition, infection of monocytes with swollen *A. fumigatus* conidia, a physiological stage of growth that results in exposure of pathogen-associated molecular patterns (PAMPs) and melanin removal from the cell wall surface[7], triggered robust CaM recruitment to the phagosome and LAPosome formation (Supplementary Fig. 1). Monocyte infection following sequential genetic removal of rodlet protein RodA (Δ*rodA*), and melanin (Δ*rodA/pksP* and Δ*pksP*) from the *A. fumigatus* conidia surface precluded a significant inhibitory effect of RodA on CaM recruitment (Fig. 1c). Genetic complementation of *pksP* fully restored the ability of melanin to block CaM recruitment and LAP (Supplementary Fig. 2). Furthermore, stimulation of monocytes with purified *A. fumigatus* melanin (melanin ghosts) completely abrogated CaM phagosome recruitment (Supplementary Fig. 3). Notably, CaM recruitment to the phagosome was also induced by other PRRs activating LAP, including FcγR (Supplementary Fig. 4).

We next performed Ca^{2+} depletion in monocytes, following a protocol of prolonged (1 h) incubation with EGTA because of the profound effect of cell-permeable Ca^{2+} chelators (1,2-bis (o-aminophenoxy)-ethane-N,N,N′,N′-tetraacetic acid acetoxymethyl ester (BAPTA-AM) or ethyleneglycol-bis(b-aminoethyl ether)-N,N′-tetraacetic acid acetoxymethyl ester (EGTA-AM)) on phagocytosis[12], and confirmed inhibition of Ca^{2+} responses (Supplementary Fig. 5a) and CaM recruitment to the phagosome of melanin-deficient conidia of *A. fumigatus* (Supplementary Fig. 5b). Importantly, Ca^{2+} depletion following prolonged EGTA treatment prevented localization of the NADPH oxidase subunits p47phox and p22phox on the phagosome (Supplementary Fig. 5c,d), abrogated ROS production (Supplementary Fig. 5e) and inhibited LAPosome formation (Supplementary Fig. 5f) in monocytes stimulated with conidia of melanin-deficient *A. fumigatus* mutants.

Treatment of monocytes with W7, a specific CaM antagonist, resulted in impaired recruitment of Rubicon (Fig. 1d,e) and VPS34 Class III PI(3)K (Supplementary Fig. 6a) to the phagosome, leading to defective PtdIns(3)P phagosomal accumulation (Fig. 1f,g) following infection with melanin-deficient *A. fumigatus* conidia. In addition, inhibition of CaM signalling compromised phagosomal localization of several NADPH oxidase subunits, p40phox (Fig. 1h and Supplementary Fig. 6b), p47phox (Supplementary Fig. 6c–e) and p22phox (Fig. 1i), and resulted in blockade in ATG7 (Supplementary Fig. 7) and LC3 recruitment to the phagosome (Fig. 1j,k). W7 treatment also blocked phagosome acidification and phagolysosomal fusion as evidenced by defective recruitment of V-ATPase (Supplementary Fig. 8a) and CD63 (Supplementary Fig 8b) to the phagosome. In contrast, inhibition of phagosomal acidification with Bafilomycin had no apparent effect on CaM recruitment (Supplementary Figure 8c).

Treatment of monocytes with a known specific calcium/calmodulin-dependent protein kinase II (CAMKII) inhibitor (KN62) abrogated *A. fumigatus* LAPosome formation (Fig. 1l). Treatment of monocytes with either W7 or KN62 resulted in attenuated killing of *A. fumigatus* conidia (Fig. 1m,n). In contrast, treatment of monocytes with cyclosporin A (CsA), an inhibitor of the calcium and calmodulin-dependent serine/threonine phosphatase calcineurin, had no apparent effect on LAP and killing of *A. fumigatus* conidia (Supplementary Fig. 9), suggesting that Ca^{2+}–CaM signalling regulating LAP is calcineurin-independent.

Notably, infection of monocytes with melanin-competent conidia of WT *A. fumigatus* paralleled the effects of inhibition of Ca^{2+}–CaM signalling on Rubicon (Fig. 1d,e) and VPS34 recruitment (Supplementary Fig. 6a), PtdIns(3)P accumulation (Figs. 1f,g), NADPH oxidase assembly (Fig. 1h,i and Supplementary Fig. 6) and LAPosome formation (Supplementary Fig. 7 and Fig. 1j,k). Collectively, our findings identify a Ca^{2+}–CaM signalling regulating Rubicon-mediated activation of NADPH oxidase and other molecular components of LAP that is inhibited by fungal melanin.

Ca^{2+}–CaM signalling depends on intracellular Ca^{2+} sources from endoplasmic reticulum. Next we sought to identify the signalling requirements for CaM localization to the phagosome. Importantly, in contrast with complete Ca^{2+} depletion following prolonged EGTA treatment (Supplementary Fig. 5), in the absence of extracellular Ca^{2+} (Ca^{2+}-free media) or following brief (5 min) pre-incubation with the cell-impermeable Ca^{2+} chelator EGTA, both CaM localization (Fig. 2a) and LAPosome formation (Fig. 2b) remained intact in monocytes stimulated with melanin-deficient *A. fumigatus*. In contrast, depletion of intracellular Ca^{2+} with the use of EGTA-AM, which was added to culture media at 10 min of infection with melanin-deficient *A. fumigatus* to allow phagocytosis, inhibited CaM recruitment (Fig. 2c) and LAP (Fig. 2d).

Furthermore, depletion of endoplasmic reticulum Ca^{2+} stores following pretreatment with thapsigargin, a sarco/endoplasmic reticulum Ca^{2+} ATPase (SERCA) inhibitor[13], abrogated CaM recruitment to the phagosome (Fig. 2e) and LAPosome formation (Fig. 2f). Notably, treatment of monocytes in Ca^{2+}-free media with increasing concentrations of lanthanum ($LaCl_3$), a general Ca^{2+} channel inhibitor, resulted in dose-dependent inhibition of CaM (Fig. 2g) and LAP (Fig. 2h). These findings suggest that Ca^{2+} is released through Ca^{2+} channels on the phagosome and that the endoplasmic reticulum regulates CaM recruitment to the phagosome and LAPosome formation.

Pharmacologically enforced cytosolic Ca^{2+} flux in monocytes/macrophages reverses phagosome maturation arrest induced by bacterial pathogens[14–16]. Therefore, we evaluated whether treatment with the Ca^{2+} ionophore ionomycin could enhance CaM recruitment to the phagosome of melanized conidia of *A. fumigatus*. Of interest, purified *Aspergillus* melanin did not impair Ca^{2+} flux triggered by ionomycin (Supplementary Fig. 10). However, cytosolic Ca^{2+} increase upon treatment with ionomycin either before or after monocyte infection with WT (melanin-competent) conidia of *A. fumigatus* failed to enhance CaM recruitment to the phagosome (Fig. 2i), implying that Ca^{2+} release from the endoplasmic reticulum to the peri-phagosomal area is not sufficient to trigger CaM recruitment.

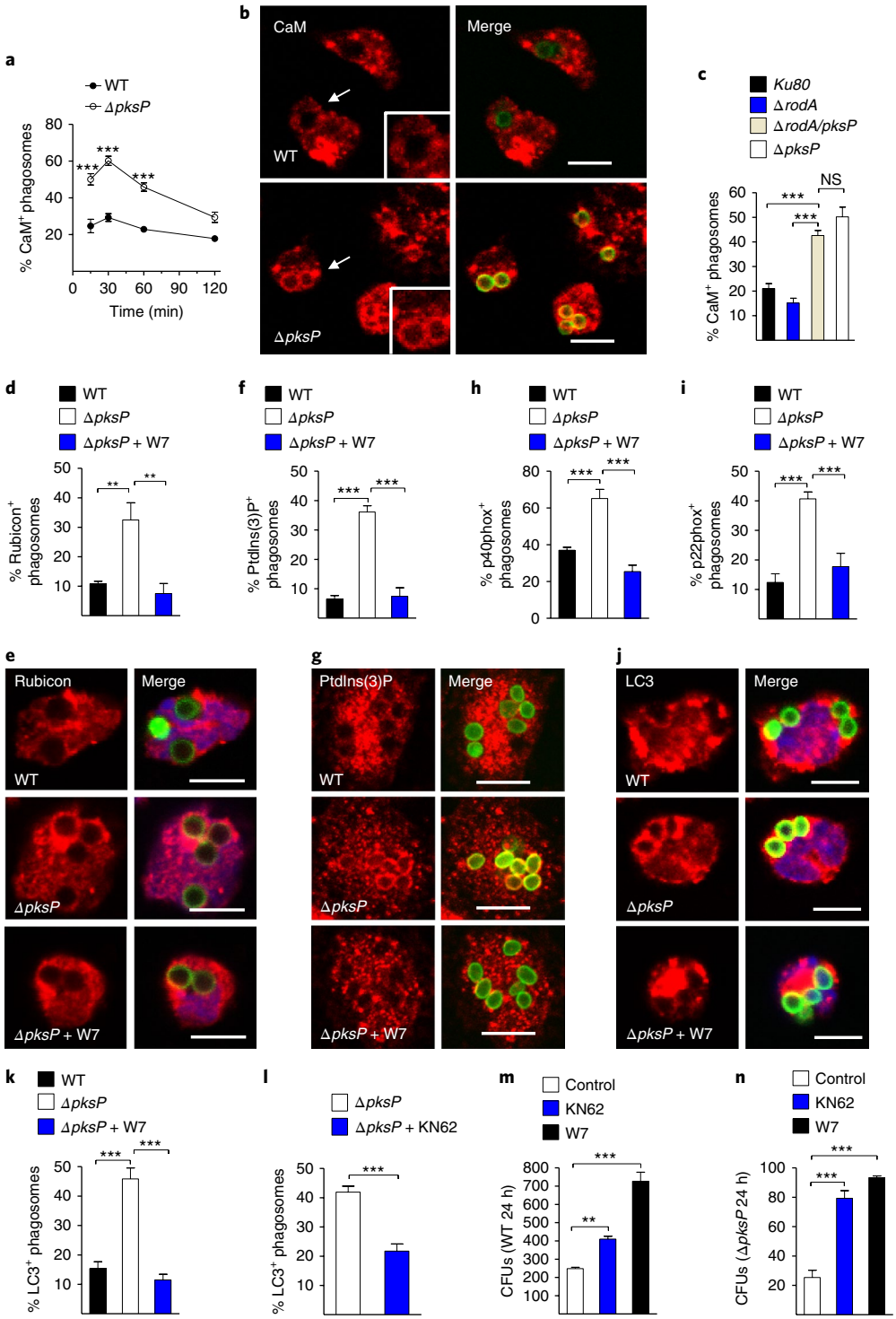

Fig. 1 | Ca^{2+}–CaM signalling regulates *A. fumigatus* LAP. a–c, Primary human monocytes were stimulated with FITC-labelled PFA killed conidia of the indicated *A. fumigatus* strain (multiplicity of infection (MOI) 3:1, 37 °C), cells were fixed at the indicated time points, stained for CaM and analysed by confocal microscopy. Data on quantification of CaM^+ phagosomes are presented as mean ± s.e.m. of four independent experiments. $^{***}P < 0.0001$, two-tailed unpaired Student's *t*-test. (**b**) Representative immunofluorescent staining for calmodulin (CaM) in primary human monocytes stimulated for 15 min as in **a**. **c**, Data on quantification of CaM^+ phagosomes stimulated with the indicated *A. fumigatus* strains for 30 min as in **a** and analysed by confocal microscopy are presented as mean ± s.e.m. of three independent experiments. $^{***}P < 0.0001$, one-way ANOVA and Tukey's multiple comparisons post hoc test. **d–l**, Primary human monocytes were infected for 30 min as in **a** with or without the presence of CaM antagonist (W7, 25 μM) added 10 min post infection (**d–k**) or the presence of CAMKII inhibitor (KN62, 10 μM) (**l**) and analysed by confocal microscopy. Data on quantification of $Rubicon^+$ (**d**), $PtdIns(3)P^+$ (**f**), $p40phox^+$ (**h**), $p22phox^+$ (**i**) and $LC3^+$ (**k**,**l**) phagosomes are presented as mean ± s.e.m. of three independent experiments. Representative immunofluorescent staining for Rubicon (**e**), PtdIns(3)P (**g**) and LC3 (**j**) are shown. $^{***}P < 0.0001$, $^{**}P < 0.001$, $^{*}P < 0.01$ two-tailed unpaired Student's *t*-test. Scale bars, 6 μm. **m**,**n**, Human monocytes were infected with either WT (**m**) or Δ*pksP* (**n**) conidia at a MOI of 1:10 (fungus:cell) with or without treatment with either W7 (25 μM) or KN62 (10 μM), both added 10 min after infection. Killing of conidia was assessed by colony-forming unit (CFU) counts at 24 h. Data are presented as mean ± s.e.m. of one out of four independent experiments performed in triplicate ($n = 3$). $^{***}P < 0.0001$, $^{**}P < 0.001$, one-way ANOVA and Dunnett's multiple comparisons post hoc test.

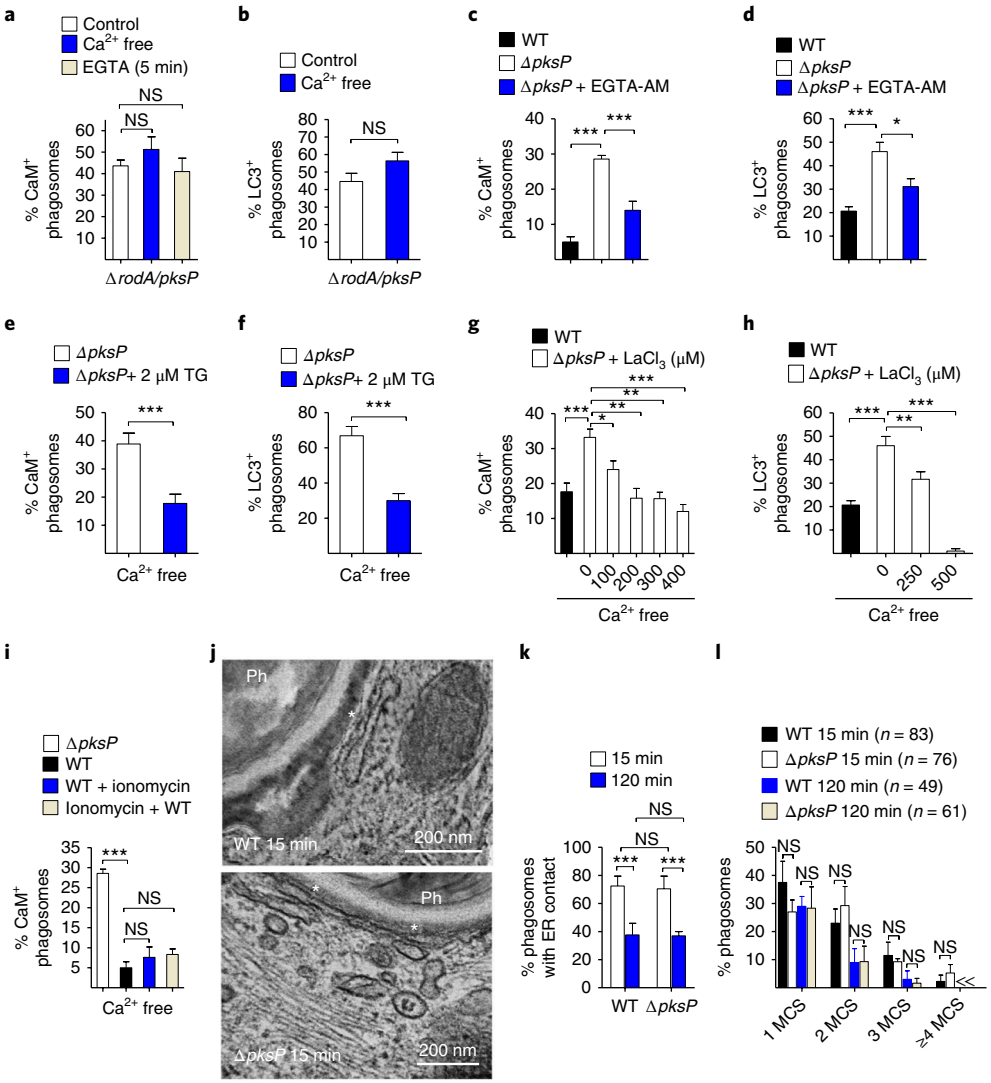

Fig. 2 | CaM phagosome recruitment is dependent on endoplasmic reticulum Ca^{2+} sources. a–i, Primary human monocytes were infected for the indicated time with FITC-labelled PFA killed conidia of the indicated *A. fumigatus* strains (MOI 3:1), in the presence or absence of chelators, inhibitors or ionomycin, and recruitment of CaM (30 min) or LC3 (60 min) to the phagosome was analysed by confocal microscopy. Where indicated infections were performed in Ca^{2+}-free medium. Depletion of extracellular Ca^{2+} was performed just before infection with the cell-impermeable chelator EGTA (500 μM). Depletion of intracellular Ca^{2+} was performed by cell-permeable chelator (EGTA-AM 500 μM) added 10 min after infection to allow phagocytosis. In certain experiments W7 (25 μM) or ionomycin (1 μM) were added 10 min post infection; TG was added 30 min before infection and $LaCl_3$ was added 15 min before infection. Data on quantification of CaM^+ (**a**,**c**) and $LC3^+$ (**b**,**d**) phagosomes in Ca^{2+}-free media or on depletion of extracellular Ca^{2+} (EGTA 5 min) or intracellular Ca^{2+} (EGTA-AM) presented as mean ± s.e.m. of three independent experiments and analysed by the two-tailed unpaired Student's *t*-test or one-way ANOVA and Dunnett's post hoc test in case of multiple comparisons. Data on quantification of CaM^+ (**e**) and $LC3^+$ (**f**) phagosomes following depletion of endoplasmic reticulum Ca^{2+} stores with TG (**e**,**f**) or upon treatment with a general Ca^{2+} channel inhibitor ($LaCl_3$) (**g**,**h**) presented as mean ± s.e.m. of three independent experiments and analysed by the two-tailed unpaired Student's *t*-test or one-way ANOVA and Tukey's post hoc test in case of multiple comparisons. **i**, Data on quantification of CaM recruitment in the phagosome of the indicated *A. fumigatus* strain upon treatment with a Ca^{2+} ionophore (ionomycin) added either before or after the infection presented as mean ± s.e.m. of three independent experiments analysed by one-way ANOVA and Tukey's multiple comparisons post hoc test $^{***}P < 0.0001$, $^{**}P < 0.001$, $^{*}P < 0{,}01$. **j**, TEM (representative of one out of three experiments repeated independently with similar results) on endoplasmic reticulum–phagosome contact following 15 min of infection of monocytes with melanin-competent or melanin-deficient conidia of *A. fumigatus*. Asterisks indicate endoplasmic reticulum–phagosome membrane contact sites (MCS). **k**,**l**, Quantitative analysis of endoplasmic reticulum–phagosome MCS at 15 min and 120 min of infection of monocytes with the indicated *A. fumigatus* strain, assessed by TEM. Data are presented as mean ± s.e.m. of pooled data from three independent experiments including four experimental conditions (WT 15 min, $n = 83$ phagosomes; WT 120 min, $n = 76$ phagosomes; Δ*pksP* 15 min $n = 49$ phagosomes; Δ*pksP* 120 min, $n = 61$ phagosomes) analysed by the two-tailed unpaired Student's *t*-test or one-way ANOVA and Tukey's multiple comparisons post hoc test. $^{***}P < 0.0001$.

In line to these findings, we found no differences in degree and kinetics of association of calnexin, a representative endoplasmic reticulum protein, with *A. fumigatus* phagosomes containing either melanin-competent (WT) or melanin-deficient (Δ*pksP*) conidia (Supplementary Fig. 11). In addition, electron microscopy studies revealed a significant and comparable degree of interaction of endoplasmic reticulum membranes with phagosomes containing either WT or Δ*pksP* conidia, which was more pronounced at early time points of monocyte infection (Fig. 2j–l). Collectively, these studies demonstrate that intracellular Ca^{2+}

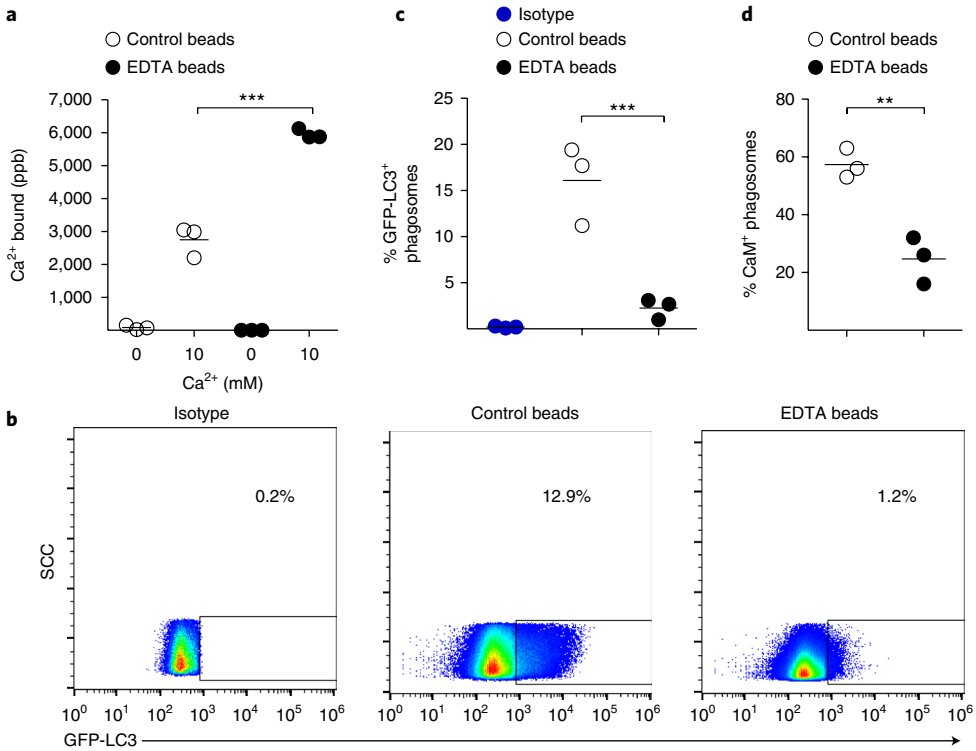

Fig. 3 | Ca^{2+} sequestration inside the phagosome abrogates CaM recruitment and inhibits LAP. a, Data on quantification of Ca^{2+} binding capacity of control magnetic beads and EDTA magnetic beads presented as mean ± s.e.m. of three independent experiments. ***$P < 0.0001$, two-tailed unpaired Student's *t*-test. Magnetic beads were incubated with increasing concentrations of Ca^{2+}, extensively washed with deionized water for removal of unbound Ca^{2+} and Ca^{2+} bound on beads was subsequently extracted by treatment with EGTA. **b**, Representative FACS analysis (Phago-FACs) of phagosomes isolated by magnetic separation from GFP-LC3 BMDMs stimulated with control magnetic beads or EDTA magnetic beads. **c**, Data on quantification of GFP-LC3$^+$ phagosomes from experiments performed in **b**. Each symbol represents an independent experiment ($n = 3$) and horizontal bars represent the mean. ***$P < 0.0001$, two-tailed unpaired Student's *t*-test. **d**, Data on quantification of CaM$^+$ phagosomes from BMDMs stimulated as in **b** and analysed with confocal microscopy presented as mean ± s.e.m. of three independent experiments. **$P < 0.001$, two-tailed unpaired Student's *t*-test.

sources from the endoplasmic reticulum and endoplasmic reticulum–phagosome communication regulate CaM recruitment. In addition, these findings suggest that melanin does not interfere with endoplasmic reticulum–phagosome association and endoplasmic reticulum Ca^{2+} release.

Ca^{2+} release from the phagosome lumen regulates CaM recruitment and LAP. To investigate the role of Ca^{2+} release from the phagosome lumen on LAP, we performed selective Ca^{2+} chelation inside the phagosome of monocytes upon phagocytosis of magnetic beads containing stably conjugated EDTA on their surface (EDTA-coated beads) or control magnetic beads (Fig. 3a). Importantly, flow cytometry analysis on isolated phagosomes from bone marrow derived macrophages (BMDMs) obtained from green fluorescent protein (GFP)-LC3 mice following stimulation with EDTA-coated beads or control beads demonstrated almost complete inhibition of GFP-LC3 accumulation to phagosomes containing EDTA-coated beads (Fig. 3b,c). In line with these findings, CaM recruitment was significantly impaired in EDTA-coated magnetic bead phagosomes as compared to the control magnetic bead phagosomes (Fig. 3d). These findings demonstrate that Ca^{2+} release from the phagosome lumen to the peri-phagosomal area is required for activation of CaM signalling regulating LAP.

Fungal melanin blocks early Ca^{2+} signalling events regulating phagosome biogenesis. In order to understand the mechanism of interference of fungal melanin with Ca^{2+} responses we performed live Ca^{2+} imaging studies in primary human monocytes preloaded with the Ca^{2+} indicator Fluo4-AM and subsequently stimulated with melanin-competent or melanin-deficient *A. fumigatus* strains. We found that phagocytosis of melanin-competent conidia of *A. fumigatus* triggered low-amplitude Ca^{2+} spikes of short duration, but failed to activate sustained cytosolic Ca^{2+} flux (Fig. 4a,b and Supplementary Videos 1 and 2). In sharp contrast, genetic removal of melanin in dormant conidia of *A. fumigatus* triggered robust and prolonged cytosolic Ca^{2+} flux during the early phase (within seconds) of phagocytosis by primary human monocytes (Fig. 4a,b and Supplementary Video 3).

In addition, we found significantly (about twofold) higher percentage of peri-phagosomal Ca^{2+} hotspots (rings) surrounding the phagosomes of melanin-deficient (Δ*rodA/pksP*) than melanin-competent (*Ku80*, Δ*rodA*) conidia of *A. fumigatus*, whereas sustained peri-phagosomal Ca^{2+} accumulation almost exclusively occurred in phagosomes of Δ*rodA/pksP* conidia (Fig. 4d,e and Supplementary Video 4).

To extend these findings further, we measured the labile (EDTA extractable) Ca^{2+} content of isolated phagosomes containing conidia of melanin-competent (WT) or the melanin-deficient (albino) Δ*pksP* isogenic mutant at different time points of infection by ICP-MS, which is indicative of the Ca^{2+} amount present in Ca^{2+}-binding proteins on the cytosolic site of the phagosome membrane[17]. Notably, we found a discordant response characterized by a sharp increase of labile Ca^{2+} in phagosomes containing melanin-deficient (Δ*pksP*) conidia as opposite to a significant decrease in labile Ca^{2+} on phagosome membranes containing melanin-competent (WT)

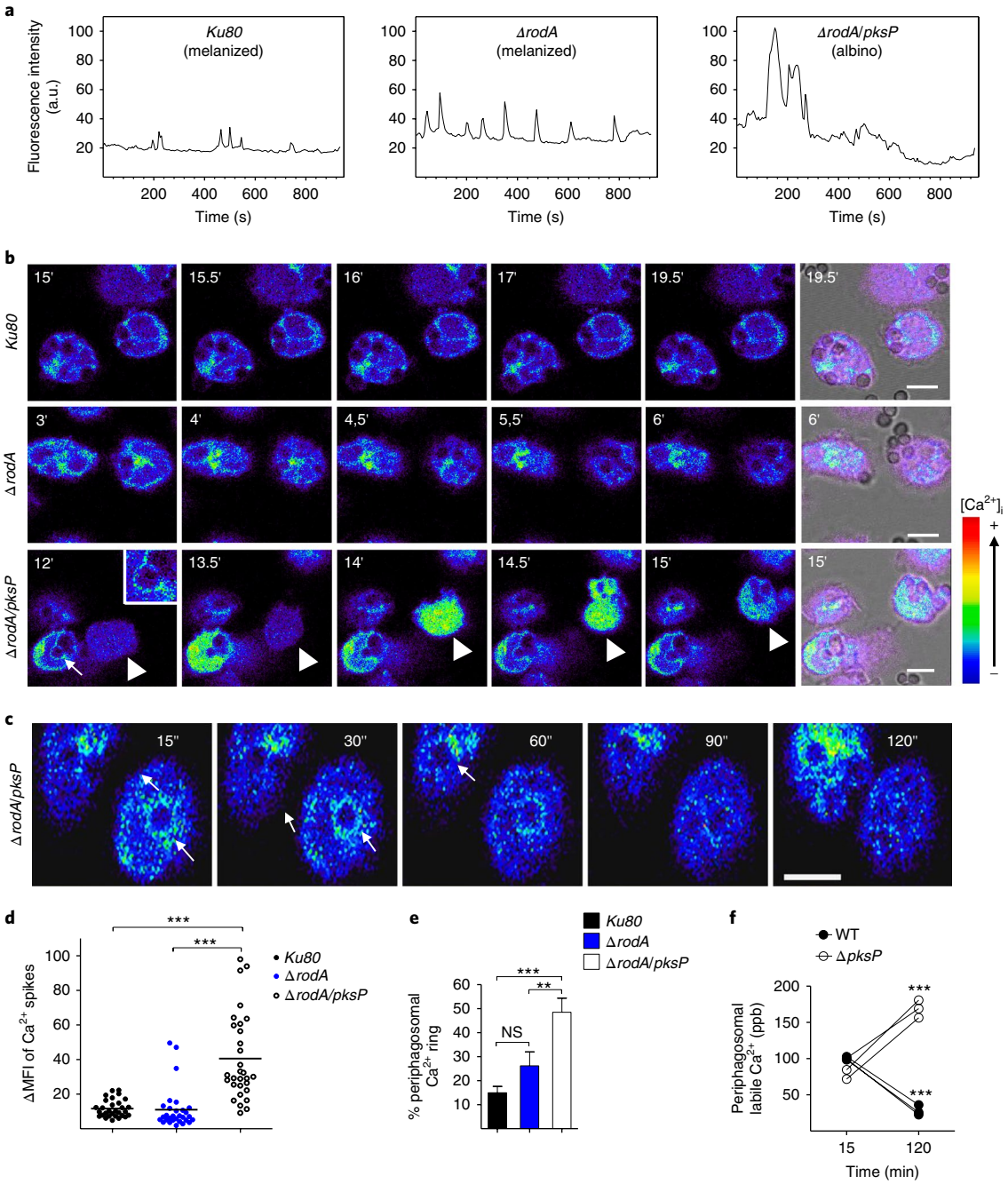

Fig. 4 | *A. fumigatus* cell wall melanin inhibits peri-phagosomal Ca^{2+} accumulation to the phagosome. a–e, Live imaging of primary human monocytes preloaded with 0.5 μM of Fluo4-AM and stimulated with PFA-inactivated conidia of melanin-competent or melanin-deficient *A. fumigatus* strain. Data from 1 out of 12 representative experiments repeated independently with similar results are shown. **a**, Representative patterns of cytosolic Ca^{2+} spikes after infection with the indicated *A. fumigatus* strains. **b**,**c**, Representative time-lapse images of general and localized Ca^{2+} responses of monocytes stimulated with melanin-competent or melanin-deficient *A. fumigatus* strains are shown. Arrows indicate peri-phagosomal Ca^{2+} rings and triangles indicate cytosolic Ca^{2+} spikes. **d**, ΔMFIs of Ca^{2+} fluxes in monocytes stimulated with *A. fumigatus* conidia of the indicated strain from 1 out of 12 experiments representative experiments repeated independently with similar results are shown. Each symbol represents ΔMFIs value of individual cell analysed ($n = 30$ cells for each condition) and horizontal bars represent the mean of ΔMFIs. Data were analysed by one-way ANOVA and Tukey's multiple comparisons post hoc test $^{***}P < 0.0001$. **e**, Data on quantification of the percentages of peri-phagosomal Ca^{2+} rings are presented as mean ± s.e.m. of pooled data from videos ($n = 3$ per condition) of two independent experiments performed with similar results, analysed by one-way ANOVA and Dunnett's multiple comparisons post hoc test $^{***}P < 0.0001$, $^{**}P < 0.001$. **f**, Accumulation of labile Ca^{2+} in phagosomes isolated at the indicated time point from human monocytes obtained from three different healthy individuals and infected with melanin-competent or melanin-deficient *A. fumigatus* strain. Ca^{2+} was extracted from phagosomes with a cell membrane impermeable chelator and measurement was performed by inductively coupled plasma mass spectrometry (ICP-MS). $^{***}P < 0.0001$, two-tailed unpaired Student's *t*-test. Scale bars, 6 μm.

conidia over time (Fig. 4f). Collectively, these studies suggest that fungal melanin blocks early Ca^{2+} signalling events regulating peri-phagosomal Ca^{2+} release, leading to impaired Ca^{2+} effector protein recruitment to the phagosome.

Ca^{2+} sequestration inside the phagosome by melanin blocks CaM recruitment and LAP. We next assessed whether Ca^{2+} sequestration inside the phagosome abrogates CaM recruitment by inhibiting luminal Ca^{2+} release to the peri-phagosomal area. We initially

compared Ca^{2+} binding properties of melanin-competent (WT) versus melanin-deficient (albino; Δ*pksP*) conidia and found that melanized conidia had a significantly (about tenfold) higher ability to sequester Ca^{2+} than the albino conidia, with the latter lacking appreciable Ca^{2+} scavenging properties even on exposure to a supra-physiological concentration of Ca^{2+} (Fig. 5a). In addition, we evaluated Ca^{2+} sequestration over time inside phagosomes isolated from human monocytes infected with either WT or Δ*pksP* conidia in the absence of extracellular Ca^{2+}. We found significant and selective accumulation of Ca^{2+} inside the phagosomes of WT conidia over time (120 min versus 15 min of infection), as opposite to the decrease of Ca^{2+} content of Δ*pksP*-containing phagosomes over time (Fig. 5b).

In order to provide further physiological evidence on the ability of Ca^{2+} sequestration by *Aspergillus* conidia to inhibit LAP, we coated PFA-inactivated melanin-deficient (Δ*pksP*) conidia with polyethylenimine (PEI), a polymer used as a linker for covalent linking of a cell-impermeable chelator (DTPA) on the conidial surface (Fig. 5c). We confirmed that both DTPA-PEI-coated Δ*pksP* conidia (hereafter DTPA-Δ*pksP* conidia) and melanized (WT) conidia had strong and comparable Ca^{2+} chelating properties as opposed to control (Δ*pksP*) conidia (Fig. 5d). Notably, the coating of Δ*pksP* conidia with PEI linked or not to DTPA did not interfere with pro-inflammatory cytokine production by monocytes (Fig. 5e). Stimulation of human monocytes with DTPA-Δ*pksP* conidia almost completely abolished CaM localization to the phagosome (Fig. 5f,g), p47phox recruitment (Supplementary Fig. 12) and LAPosome (Fig. 5h,i) formation when compared with stimulation with control (Δ*pksP* or PEI-coated Δ*pksP*) conidia, at levels similar to that observed upon stimulation with melanin-competent (WT) conidia. These studies demonstrate that Ca^{2+} sequestration induced by fungal melanin inside the phagosome lumen is the predominant mechanism of inhibition of Ca^{2+}–CaM signalling regulating LAP (Supplementary Fig. 13).

Impaired Ca^{2+}–CaM signalling results in heightened susceptibility for invasive *Aspergillosis* in haematopoietic stem-cell transplant recipients. Taken together, our data suggested that Ca^{2+}–CaM signalling could play a key role in immunity to infection with *Aspergillus*. Therefore, we next explored the role of this pathway in humans. A functional single nucleotide polymorphism (SNP) in the core promoter of the calmodulin I gene (rs12885713) was reported to decrease transcription in vitro and in vivo[18]. Remarkably, we found a highly significant association between this SNP (CALM1 CC recipient genotype) and the risk of aspergillosis (Fig. 6) in a cohort of haematopoietic stem-cell transplant recipients[19]. In a multivariate model accounting for clinical variables associated with or tending towards invasive aspergillosis in our cohort, the only independent predictors of invasive aspergillosis were severe acute graft-versus-host disease (HR 2.24, 95% CI 1.14–4.93; $P=0.012$) and the CC recipient genotype at rs12885713 on CALM1 (HR 2.2, 95% CI 1.08–4.87; $P=0.024$) (Supplementary Table 1). The CALM1 CC recipient genotype had no impact in overall survival (Supplementary Fig. 14a) and did not affect lung cytokine responses measured in the bronchoalveolar lavage of available patients (Supplementary Fig. 14b). Although the functional significance of CALM1 CC genotype on recipient antifungal host defence requires further exploitation, these data suggest a pathogenetic role for impaired Ca^{2+}–CaM signalling in human fungal disease.

Discussion

LAP is a non-canonical autophagy pathway with central role in host defence against an expanding list of other human pathogens[2,3,7,8,20–22]. The signalling regulating LAP is distinct than that of general (macro) autophagy and has not been fully elucidated[1,2]. Although Ca^{2+}–CaM signalling is a master regulator of macroautophagy[11], there are no previous implications for a role of Ca^{2+} signalling in LAP. Notably, previous studies demonstrated that Ca^{2+}–CaM/CAMKII signalling regulates the early steps of phagosome biogenesis and is targeted by *Mycobacterium tuberculosis*[15,23]. Nonetheless, the Ca^{2+} source and mechanism of CaM recruitment to the phagosome and a link of this pathway with LAP have not been previously identified.

Herein, we identify intracellular endoplasmic reticulum Ca^{2+} and peri-phagosomal Ca^{2+} release from the phagosome lumen as the master regulators of CaM dependent activation of LAP responses to *Aspergillus* in monocytes/macrophages. In neutrophils, peri-phagosomal Ca^{2+} domains regulate respiratory burst, phagolysosomal fusion, degranulation and other essential effector functions[24,25] in a process that depends on extracellular Ca^{2+} via store-operated Ca^{2+} entry[26]. In other phagocytes, including monocytes/macrophages, there is conflicting evidence on role of Ca^{2+} signalling in phagosome responses[10]. Our findings on the major role of intracellular Ca^{2+} sources from endoplasmic reticulum on phagosome biogenesis and LAP extend on recent studies demonstrating the important role of endoplasmic reticulum–phagosome communication and peri-phagosomal Ca^{2+} release in membrane fusion events during phagocytosis[1,28–30].

Although Ca^{2+} is involved in zymosan-induced ROS production in monocytes/macrophages[31,32], the role of Ca^{2+}–CaM signalling on regulation of NADPH oxidase assembly has not been previously explored. Stabilization of NADPH oxidase complex on the phagosome is regulated by Rubicon-dependent activation of VPS34 class III PI(3)K via sustained PtdIns(3)P production and direct interaction with the PX [PtdIns(3)P binding] domain of p40phox subunit[2]. In addition, Rubicon directly interacts with p22phox subunit and facilitates NADPH oxidase activation during phagocytosis of zymosan, a physiological ligand of PRRs prepared from yeast cell wall[33]. Herein, we found that Ca^{2+}–CaM signalling is an upstream regulator of Rubicon–VPS34 class III PI(3)K phagosomal localization, PtdIns(3)P production, NADPH oxidase activation and LAP (Supplementary Fig. 13). These findings provide insight on the mechanisms of melanin-induced inhibition of NADPH oxidase assembly and pave the way for future studies on identification and in vivo validation of the molecular components of Ca^{2+}–CaM signalling regulating LAP upstream of Rubicon.

It is plausible that during the complex and dynamic process of phagosome biogenesis communication of the phagosome with intracellular Ca^{2+} sources other than the endoplasmic reticulum, and/or endoplasmic reticulum–mitochondria communication[34] (Supplementary Fig. 15) could amplify Ca^{2+} responses on the phagosome[35]. In addition, despite the dispensable role of store-operated Ca^{2+} entry in phagosome functions of monocytes/macrophages[36], identification of the full spectrum of Ca^{2+} channels mediating endoplasmic reticulum–phagosome communication and peri-phagosomal Ca^{2+} release should be an important future direction.

Other than regulating pathogen killing, activation of LAP in macrophages and dendritic cells has an important anti-inflammatory function both at the steady state and during *A. fumigatus* infection[3–5,8,9]. Ca^{2+} signalling in resident myeloid cells also orchestrate inflammatory responses in the lung[37,38]. Therefore, it is tempting to speculate that Ca^{2+}-dependent activation of LAP is involved in regulation of inflammation and immunity in the lung.

Melanins are ubiquitous, heterogeneous macromolecules of incompletely characterized composition, structure[39–41]. Metal chelation is a common characteristic of melanins and Ca^{2+} sequestration has been described in all melanized tissues of the human body[40–47]. However, no clear biological function of the Ca^{2+} binding properties of melanin has been previously described. Our study links Ca^{2+} chelating properties of melanins with immunomodulation, and provides mechanistic explanation on the common ability of these molecules to target the LAP pathway. Future studies should also explore the role of metal binding properties of melanin on the function of Ca^{2+} channels and other divalent cation transporters.

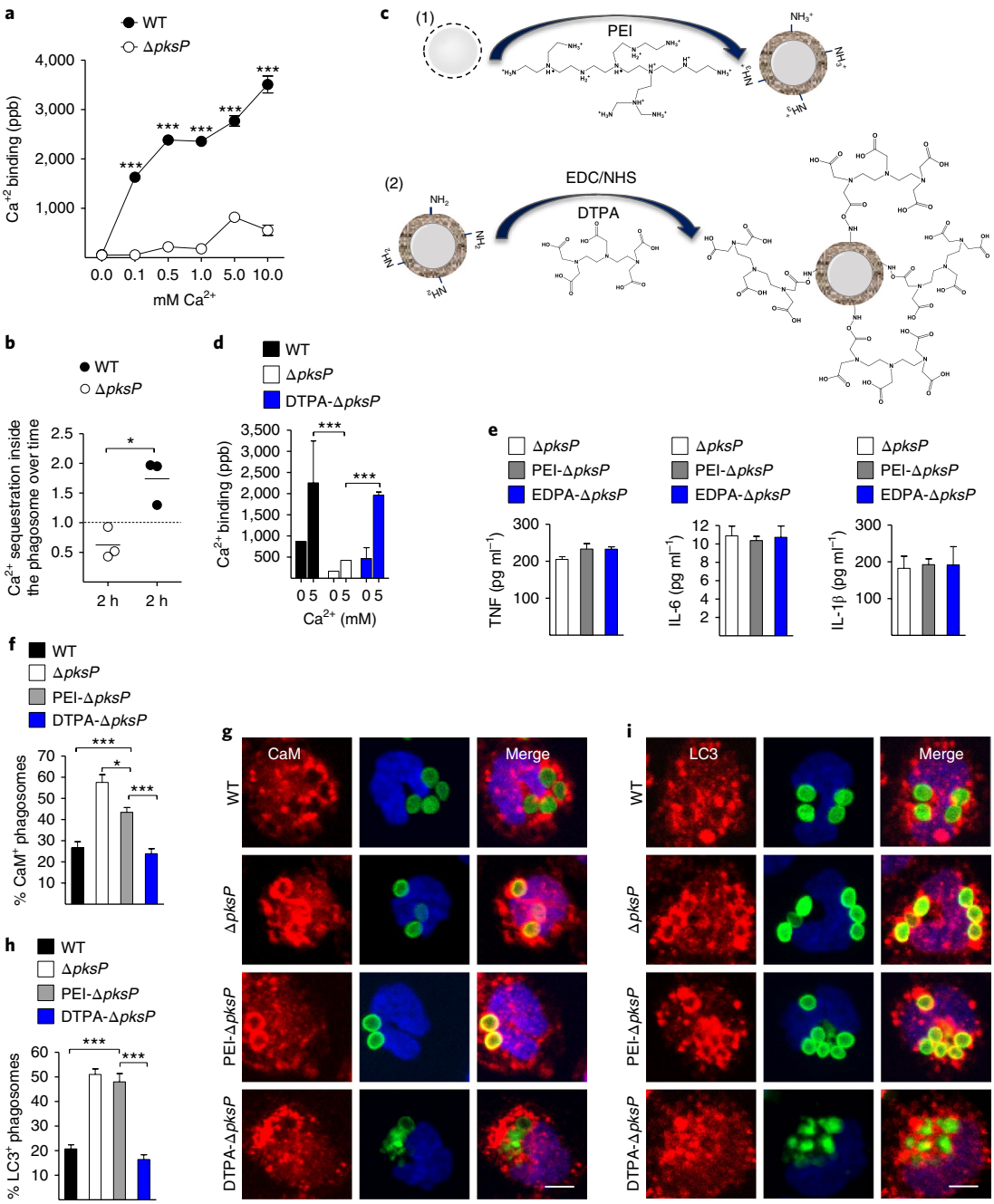

Fig. 5 | Ca^{2+} sequestration by melanin inside the phagosome blocks CaM dependent activation of LAP. a, Data on quantification of Ca^{2+} binding capacity of melanin-competent (WT) and melanin-deficient (Δ*pksP*) conidia of *A. fumigatus* presented as mean ± s.e.m. of four independent experiments. ***$P < 0.0001$, two-tailed unpaired Student's *t*-test. **b**, Ca^{2+} sequestration inside phagosomes (10^7 per condition) isolated at different time points (15 min, 120 min) of infection of primary human monocytes with melanin-competent (WT) and melanin-deficient (Δ*pksP*) conidia in Ca^{2+}-free media. Ca^{2+} sequestration at 120 min of infection was normalized to the phagosome Ca^{2+} content present at 15 min of infection. Mean values are represented with horizontal bars. *$P < 0{,}01$ two-tailed unpaired Student's *t*-test. **c**, Schematic illustration of the electrostatic coating of Δ*pksP* conidia with polyethylenimine (PEI) (1), followed by the covalent linking of the Ca^{2+} chelator DTPA to PEI using EDC/NHS (2). **d**, Data on quantification of Ca^{2+} binding capacity of the indicated conidia of *A. fumigatus* measured as in **a**, presented as mean ± s.e.m. of four independent experiments. ***$P < 0.0001$, two-tailed unpaired Student's *t*-test. **e**, Cytokine production following overnight stimulation of human monocytes (10^5 per condition) with the indicated conidia presented as mean ± s.e.m. of three independent experiments. **f-i**, Data on quantification of CaM^+ (**f**,**g**) and $LC3^+$ (**h**,**i**) phagosomes in monocytes stimulated in Ca^{2+}-free media with the indicated *A. fumigatus* conidia and analysed by confocal imaging are presented as mean ± s.e.m. of three independent experiments. Representative images of CaM (**g**) and LC3 (**i**) recruitment are shown. ***$P < 0.0001$,**$P < 0.001$, two-tailed unpaired Student's *t*-test. Scale bars, 4 µm.

From the pathogen perspective, it would be interesting to explore the effect of metal binding by cell wall melanin on activation of Ca^{2+} signalling pathways regulation proliferation and survival of the fungus during infection (Supplementary Fig. 16).

Importantly, inhibition of Ca^{2+} signalling responses during phagocytosis is a well-defined virulence strategy of intracellular pathogens[14–16,24,48,49]. Furthermore, certain Ca^{2+}-binding proteins of bacterial and fungal pathogens act as virulence factors[50,51]. However,

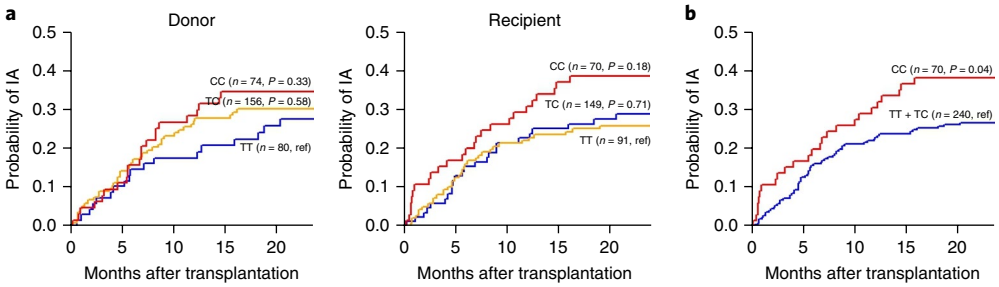

Fig. 6 | CALM1 gene polymorphism CC is associated with increased risk for invasive aspergillosis in a high-risk group of haematopoietic stem-cell recipients. Cumulative incidence of invasive aspergillosis (IA) and overall survival estimate at 36 months after haematopoietic stem cell transplantation according to CALM1 CC genotype in donor and recipient. The probability of invasive pulmonary aspergillosis according to *CALM1* genotypes was determined using the cumulative incidence method and compared using Gray's test (two-tailed). Cumulative incidences of infection were computed with the *cmprsk* package for R version 2.10.1, with censoring of data at the date of last follow-up visit and relapse and death as competing events.

our study is the first to directly demonstrate that Ca^{2+} sequestration by a microbial factor inside the phagosome inhibits essential phagocyte effector functions to promote virulence. In addition, it would be important to explore the immunomodulatory role of melanin on macrophage Ca^{2+} responses and LAP during the process of wound healing, malignancy and chronic inflammation[52–55].

Collectively, our work identifies an antifungal host defence pathway regulated by Ca^{2+}–CaM signalling and reveals that Ca^{2+} sequestration by melanin has an important pathogenetic role in development of fungal diseases. In view of the physiological importance of both melanins and the LAP pathway in humans, our findings have broader implications in the pathogenesis of diseases beyond fungal infections.

Methods

Reagents. The following antibodies and inhibitors were used for ex vivo studies in human and murine primary monocytes/macrophages: Thapsigargin (T9033, Sigma-Aldrich), CGP 37157 (C8874, Sigma-Aldrich), EGTA-AM (sc-203937, Santa Cruz Biotechnology), W7 (A3281, Sigma-Aldrich), KN62 (422706, Calbiochem), Bafilomycin A1 (B1793, Sigma-Aldrich), Cyclosporin A (C3662, Sigma-Aldrich), Fluo-4AM (F14201, Molecular Probes), Ionomycin (I0634, Sigma-Aldrich), Bapta-AM (196419, Calbiochem), Pluronic F-127 (P2443, Sigma-Aldrich), BMag Silica-Modified Magnetic Beads and BMag EDTA Magnetic Beads 1 µm diameter (Bioclone), a-calmodulin (MA3-917, ThermoFisher Scientific; dilution 1:50), a-calmodulin (NBP1-61548, Novus; dilution 1:100), a-LC3B (clone 5F10, Nanotools; dilution 1:20), a-Rubicon (ab156052, Abcam; dilution 1: 50), a-Vps34 (4263, Cell Signalling; dilution 1:20), a-PI(3)P (Z-P003, Echelon; dilution 1:100), a-p22phox (sc-20781, Santa Cruz; dilution 1:100), a-p47phox (610354 BD; dilution 1:100), a-p40phox (clone D8, sc-48388, Santa Cruz; dilution 1:100), a-ATG7 (ab133528; Abcam; dilution 1:50), rabbit polyclocal anti-GFP (Minotech Biotechnology, Heraklion, Greece; dilution 1:500), a-VATPase (ATP6V1B2; 73404, Abcam; dilution 1:100). The specific reagents used to generate DTPA-PEI-coated *Aspergillus* conidia were polyethylenimine (PEI; 408727, Sigma-Aldrich), diethylenetriaminepentaacetic acid (DTPA; D6518, Sigma-Aldrich), MES hydrate (69890, Sigma-Aldrich), *N*-(3-dimethylaminopropyl)-*N′*-ethylcarbodiimide hydrochloride (EDC; 03450, Sigma-Aldrich) and *N*-hydroxysuccinimide (NHS; 130672, Sigma-Aldrich), hydrochloric acid (HCl; 20252, VWR International) and sodium hydroxide (NaOH; S/4920/60, Fisher Chemical).

For the ICP-MS quantification of Ca^{2+} the following reagents were used: trace metal grade nitric acid, trace metal grade hydrogen peroxide 30% (Fisher Scientific). The calcium standard and a mixture of scandium, indium, yttrium and bismuth were from High-Purity Standards.

Microorganisms and culture conditions. All *A. fumigatus* strains used (Δ*pksP* and the isogenic WT strain ATCC46645; Δ*rodA*, Δ*rodA/pksP* generated on the *Ku80* background) have been described previously[7]; generation of the Δ*pksP* mutant on the *Ku80* background was performed with the 4813 bp DNA construct, already described for the double mutant ΔrodA/pksP[7]. Transformation was performed by electroporation on conidia of the CEA17_ΔakuB^{KU80} parental strain (Supplementary Fig. 17). *A. fumigatus* B-5233 (WT parental strain), B-5233/RGD12-8 (Δ*pksP*) and RGD12-8/PKS33-3 (*pksP*-complemented) strains were used in studies on *pksP* complementation[56] All strains were grown on YAG agar plates for 3 days at 37 °C. Fungal conidia (spores) were harvested by gentle shaking in the presence of sterile 0.1% Tween 20 in PBS, washed twice with PBS, filtered through a 40-µm-pore cell strainer (Falcon) to separate conidia from contaminating mycelium, counted by a haemocytometer, and suspended at a concentration of 10^8 spores ml^{-1}. When indicated, the conidia were labelled with FITC or Alexa^{647} succinic ester dye (Invitrogen) as previously described[6,7]. Briefly, freshly harvested conidia (5×10^7 per 2 ml of 50 mM Na carbonate buffer, pH 10.2) were incubated with FITC (final concentration, 0.1 mg ml^{-1}) or Alexa^{647} succinic ester dye (Invitrogen) at 37 °C for 1 h and washed by centrifugation three times in PBS–0.1% Tween 20. Inactivation of fungal conidia was done by exposure to 4% PFA (2 h, room temperature) following by treatment with glycine (100 mM in PBS) and three washes in PBS and verified by c.f.u. plating. Importantly, we have previously validated that PFA inactivation of *A. fumigatus* conidia does not affect surface exposure of β-glucan, Dectin-1 signalling activation, cytokine responses and melanin inhibitory action on LAP[6,7]. In addition, pilot experiments on Ca^{2+} signalling responses in monocytes were also performed with live *A. fumigatus* conidia.

***A. fumigatus* melanin extraction.** The isolation of melanin from wild-type (*Ku80*) conidia was performed as previously described[7]. Briefly, conidia were treated with a combination of proteolytic (proteinase K; Sigma) and glycohydrolytic (Glucanex; Novo) enzymes, denaturant (guanidine thiocyanate) and hot, concentrated HCl (6 M). This treatment resulted in an electron-dense layer similar in size and shape to the original conidial melanin layer without underlying cell components, for which reason these electron-dense materials were called 'melanin ghosts'.

Isolation and stimulation of primary human monocytes. Healthy volunteers without any known infectious or inflammatory disorders donated blood. Monocytes from healthy controls were isolated from PBMCs using magnetic bead separation with anti-CD14 coated beads (MACS Miltenyi) according to the protocol supplemented by the manufacturer. The monocytes were resuspended in RPMI culture medium supplemented with gentamicin 1%, L-glutamine 1% and pyruvate 1%. The cells were counted in a Bürker counting chamber, and their number was adjusted to 2×10^6 ml^{-1}. A total of 1×10^5 monocytes per condition in a final volume of 200 µl were allowed to adhere to polylysine treated glass coverslips (Ø 12 mm) for 1 h followed by stimulation with *A. fumigatus conidia* at a multiplicity of infection (MOI) of 3:1 at 37 °C for the indicated time point. After stimulation, cells were washed twice with PBS to remove medium and non-phagocytosed spores and cells were fixed on the coverslips for 15 min in 4% paraformaldehyde. Subsequently the coverslips were washed with PBS followed by a fixation in ice cold methanol for 10 min at −20 °C after which cover slips will be stored in PBS at 4 °C until immunofluorescence staining.

Immunofluorescence staining. For immunofluorescence imaging, cells were seeded on coverslips pretreated with polylysine, fixed with 4% PFA for 15 min in room temperature following by 10 min of fixation with ice cold methanol at −20 °C, washed twice with PBS, permeabilized by using 0.1% saponin (Sigma-Aldrich), blocked for 30 min in PBS-BSA (PBS + 2% BSA), incubated for 1 h with the indicated primary antibody, washed twice in PBS-BSA, stained by the appropriate secondary AlexaFluor secondary Ab (Molecular Probes), followed by DNA staining with 10 µM TOPRO-3 iodide (642/661; Invitrogen). After the washing steps, slides were mounted in Prolong Gold antifade media (Molecular Probes). Images were acquired using a laser-scanning spectral confocal microscope (TCS SP2; Leica), LCS Lite software (Leica), and a 40× Apochromat 1.25 NA oil objective using identical gain settings. A low fluorescence immersion oil (11513859; Leica) was used, and imaging was performed at room temperature. Serial confocal sections at 0.5 µm steps within a z-stack spanning a total thickness of 10–12 µm of the cell were taken and three-dimensional images were generated using the LCS Lite software to assess for internalized conidia contained within phagosomes. Unless otherwise stated, mean projections of image stacks were obtained using the LCS Lite software and processed with Adobe Photoshop CS2.

Phagosomes surrounded by a rim of fluorescence of the indicated protein marker were scored as positive, according to established protocols in our laboratory. At least 200 phagosomes were analysed for each experimental condition in three independent experiments.

Ca^{2+} live imaging. Primary human monocytes were loaded with the calcium indicator FLUO-4-AM (5 μM final concentration, Invitrogen) according to the manufacturer protocols. Briefly, monocytes were placed in serum free HBSS (without Ca^{2+}, without red phenol, 1 mM $MgCl_2$, 20 mM Hepes) and loaded with FLUO-4 AM in the presence of 0.02% pluronic acid for 30 min at room temperature. Then, cells were washed three times with ice cold PBS, counted and seeded in chambers for live imaging (627870 Greiner) in HBSS (without red phenol, 2 mM $CaCl_2$, 1 mM $MgCl_2$, 20 mM Hepes). After adhesion of the cells, infections with the indicated *A. fumigatus* strain or *A. fumigatus* purified melanin were performed just before live imaging followed by treatment with appropriate inhibitors. Acquisition was performed in SP8 Lieca converted microscope with 40× Apochromat 1.25 NA water objective using identical imaging setting and high-speed live imaging with the use of resonant scanner.

Measurement of ROS production. ROS measurements were performed by means of a dichlorofluorescein assay[6,7]. Stock solution of dichlorofluorescein diacetate (DCFH-DA) were dissolved in dimethyl sulfoxide (DMSO) to a final concentration of 100 mM. Human monocytes (2×10^5 per well) were plated on 96-well round bottom plates, incubated at 37 °C for 30 min and stimulated for 1 h with *A. fumigatus* conidia of the indicated strain in the presence of DCFH-DA added to a final concentration of 10 μM during the last 30 min. After 30 min of exposure, the content of the wells was transferred to vials and the fluorescence of the cells from each well measured by flow cytometry. Cells were acquired on a FACSCalibur (BD Biosciences) and analysed using FlowJo software (Tree Star).

Generation of murine BMDMS. C57BL/6 mice obtained from the IMBB Institute (Crete), and GFP-LC3 mice (obtained from RIKEN BioResource Center) were maintained in grouped cages in a high-efficiency particulate air-filtered environmentally controlled virus-free facility (24 °C, 12/12 h light/dark cycle), and fed a standard chow diet and water ad libitum. All experiments were approved by the local ethics committee of the University of Crete Medical School, Greece, in line with the corresponding National and European Union legislation.

BMDMs were generated by culturing BM cells obtained from 8-week-old female mice in DMEM, supplemented with L929 cell-conditioned medium (30%). The resulting cultures consisted of macrophages (>95% purity), as determined by staining for F4/80 and flow cytometry.

Isolation protocol of *Aspergillus*-containing phagosomes. We used an established protocol for isolation of phagosomes from primary monocytes stimulated with *A. fumigatus* conidia[7]. For measurement of Ca^{2+} sequestration inside the phagosome, monocytes (1×10^7 per condition) were stimulated in zero (0) Ca^{2+} conditions in 6 well plates with conidia of the indicated *A. fumigatus* strain at a MOI of 1:10 on ice for 30 min to synchronize phagocytosis and then allowed to phagocytose for different time points at 37 °C. Next, cells were washed three times with PBS, scraped with rubber policeman and centrifuged at 200*g* for 5 min at 4 °C. Cell pellets were resuspended in 1 ml of homogenization buffer (250 mM Sucrose, 3 mM Imidazole, pH 7.4) containing a protease inhibitor mixture without EDTA (Thermo) and cell lysis was performed on ice by passing the cell suspensions 60 times through a 28G syringe needle. Cell breakage was checked with microscopic observation and the homogenates were incubated with 10 mM ATP for 15 min with rotation in cold room in order to release the rigor mortis actin–myosin interaction. Afterwards the homogenates containing fungal phagosomes were layered over 500 μl Ficoll and centrifuged at 560*g* for 20 min. After centrifugation the pelleted conidia containing phagosomes were washed twice with PBS, phagosomes were counted and adjusted in equal numbers (5×10^7 phagosomes per condition) and used for ICP-MS.

For isolation of magnetic bead-containing phagosomes we followed the protocol described above and the final step of phagosome isolation was performed with magnetic isolation.

Endoplasmic reticulum Ca^{2+} store depletion. Freshly isolated primary human monocytes were incubated for 30 min at 37 °C with different concentrations of Thapsigargin for Ca^{2+} depletion of endoplasmic reticulum, in RPMI complete medium (10 mM Hepes, 1 mM sodium pyruvate, 25 mM glucose, 10% FCS, 2 mM L-glutamine, 0.05 mM 2-mercaptethanol, penicillin/streptomycin). Just before infection RPMI was substituted with HBSS without Ca^{2+} (1 mM $MgCl_2$, 20 mM Hepes) and infections were performed in the absence of Ca^{2+}.

Ca^{2+} channel inhibition. Freshly isolated primary human monocytes were incubated for 15 min with different concentrations of $LaCl_3$ at 37 °C in RPMI complete medium. Subsequently culture medium was substituted with HBSS without Ca^{2+} (1 mM $MgCl_2$, 20 mM Hepes) and infections were performed in the absence of Ca^{2+}.

Western blot analysis. Human monocytes were stimulated with PFA killed *Aspergillus fumigatus* conidia or magnetic beads for the indicated time points at a MOI 10:1. Cells were washed once in PBS prior to lysis in 1% NP-40 containing RIPA buffer (50 mM Tris, pH 7.4, 150 mM NaCl, 1 mM EDTA, 0.25% sodium deoxycholate, 1 mM NaF, 1 mM Na_3VO_4, 1 mM PMSF plus a mixture of protease inhibitors (Roche Molecular Biochemicals)). Cell lysis was performed on ice for 20 min and samples were centrifuged. After protein estimation of supernatants, addition of SDS sample buffer and boiling, samples were separated on SDS–PAGE and transferred to polyvinylidene difluoride (PVDF) membranes. Western blotting was performed according to the instructions of the manufacturer using the indicated primary and secondary antibodies. The blots were developed using chemiluminescence (Luminata, Millipore). WB analysis will be similarly performed in phagosome protein extracts.

Measurement of cytokines. Supernatants of stimulated human monocytes were collected after overnight culture. Cytokine levels in the supernatants were determined by using ELISA kits for human IL-1β, IL-6 and TNF (eBioscience) according to the manufacturer's instructions.

RNA extraction and qPCR. RNA from *A. fumigatus* Δ*Ku80* and Δ*pksP* was isolated at different time points after infection of human monocytes using 400 μl AE buffer pH 5.0 (50 mM sodium acetate, 10 mM EDTA), 40 μl SDS 10% (w/v) and 400 μl acidic phenol pH 4.5), and disruption with 0.5 mm silica beads in a Bead Beater apparatus at high-speed setting (5 pulses of 4 m s^{-1} for 20 s). To guarantee conidial lysis, the cellular suspension was warmed up at 65 °C for 5 min and frozen at −80 °C for at least 15 min. The colourless upper aqueous phase (containing RNA) obtained upon centrifugation at 12,000*g* (10 min at RT) was collected and mixed with 0.1 volume of sodium acetate pH 5.2 and 2 volumes of cold ethanol 70% (v/v). After centrifugation, the RNA pellet was washed with cold ethanol 70% (v/v) and centrifuged again at 7,500*g* (5 min). The air-dried RNA pellet was dissolved with RNAse-free water, and the quantity and quality of the extracted RNA were assessed by determining the A260 nm/A280 nm ratio (NanoDrop), as well as by electrophoresis in a 1.5% agarose gel for the presence of intact 18S and 28S ribosomal RNA bands by UV transillumination.

Relative mRNA expression levels of *CrzA1* were determined by qRT–PCR. One microgram of total RNA was reverse transcribed using cDNA Reverse Transcription Kit (NZYTech). Real-time RT–PCR was performed in an Applied Biosystems 7500 Fast PCR system (Thermo Fisher) using PowerUp SYBR Green Master Mix (Applied Biosystems). PCR primers for *CrzA1* were: sense, 5′-CGACTTCTCCGCAGATCTCC-3′ and antisense, 5′-CTGCCAGTCAGGATGTGTGT-3′. The thermal profile was 50 °C for 2 min for uracil-DNA glycosylase activation, 95 °C for 2 min followed by 40 cycles of denaturation for 3 s at 95 °C, and an annealing/extension step of 30 s at 60 °C. Amplification efficiencies were validated, and the expression of the target gene value was normalized against the expression of the β-tubulin gene. Gene expression was calculated using $2^{-\Delta\Delta CT}$ method relative to the unstimulated sample.

Killing of *A. fumigatus* by primary human monocytes. Primary human monocytes (2×10^5 per well) were plated onto 96-well round bottom plates for 1 h, and subsequently infected with the indicated *A. fumigatus* strain at a MOI of 1:10 (conidia: monocyte ratio) for 1 h at 37 °C with or without the presence of CaM antagonist W7 (25 μM), CAM KII inhibitor KN62 (10 μM), or Cyclosporin A (CsA; 1000 ng ml^{-1}), all added 10 min post infection. Medium containing non-adherent, non-phagocytosed conidia was removed, wells were washed three times using warm PBS, and new media with or without the presence of the corresponding inhibitor were added. Monocytes were then allowed to kill conidia for 24 h before intracellular conidia were harvested by lysis of monocytes with 0.5% Triton-X. The process of cellular lysis was confirmed by light microscopy and killing of *A. fumigatus* conidia was assessed by c.f.u. plating. Each condition was performed in quadruplicate with monocytes obtained from 4 different donors.

Transmission electron microscopy. Primary human monocytes were stimulated on Melinex coverslips (Agar Scientific), fixed with 2.5% glutaraldeyde, in 0.09 M sodium cacodylate buffer (SCB), pH 7.2, containing 3 mM Ca_2Cl for 30 min (RT), and washed with 0.1 M SCB 3×10 min. The obtained monolayers were post-fixed in cacodylate-buffered 1% OsO_4 for 2 h, dehydrated and embedded in Epon 812 (Merck). An ultratome (Leica, Reichert Ultracuts) was used to cut ultrathin sections, which were contrasted with 4% uranyl acetate for 45 min and lead citrate for 4 min at room temperature. Finally, the sections were examined using a Jeol 1200 EX2 electron microscope (JEOL, Tokyo, Japan). Quantification of endoplasmic reticulum–phagosome membrane contact sites (MCS) was conducted in single-blind and performed manually. MCS were defined as areas where the endoplasmic reticulum was <30 nm away from the phagosomal membrane, as previously described[27,29]. Phagosome cross-sections smaller than 1.5 μm in diameter were excluded from the analysis to avoid any under-sampling bias of phagosomal membranes.

Ion chromatography analysis for assessment of Ca^{2+} binding affinity of conidia of melanin-competent (wild type) and melanin-deficient (Δ*pksP* mutant) *A. fumigatus strains*. A 2×10^8 sample of PFA-inactivated conidia of the indicated strain were incubated overnight with 1 ml of 50 mM EDTA pH 8.0. Conidia were washed twice with nanopure water (>18.2 MX) obtained from a Millipore Simplicity TM system (Millipore) incubated overnight with 10 mM $CaCl_2$, pH 7.0, washed twice with nanopure water and Ca^{2+} bound on the cell wall surface were extracted following overnight incubation with 10 mM EGTA. The Ca^{2+} concentration was determined with the use of ion chromatography. The analysis system consisted of a Marathon IV HPLC pump connected with a Dionex Conductivity Detector CDM-2, two columns, Dionex CS12a (4×250 mm^2) coupled with the corresponding guard CG12a (4×50 mm^2) and a Electrolytically Self Regenerated Suppressor, Dionex CERS 500×4 mm^2. The elution was isocratic and the eluent was methanesulfonic acid (MSA) 20 mM. The retention time for Ca^{2+} was about 14 min.

Measurements of labile Ca^{2+} bound on phagosome membrane and the Ca^{2+} content of isolated phagosomes. Primary human monocytes (2×10^6 cells per condition) were stimulated in Ca^{2+}-free media with PFA-inactivated conidia of melanin-competent (WT) or melanin-deficient (Δ*pksP*) *A. fumigatus* at a 1:10 MOI and phagosomes were isolate at different time points. The Ca^{2+} content of phagosomes was extracted and measured with the use of established protocols[17]. Briefly, *Aspergillus*-containing phagosomes were reconstituted in 500 ml of deionized water and enumerated using a haemocytometer. Equal amounts of phagosomes were subjected to 5 s sonication followed by incubation with the cell membrane impermeable chelator EDTA for extraction of the labile Ca^{2+} fraction. Next, phagosomes were sonicated for 30 min and processed by an acid digestion protocol with trace metal grade nitric acid and trace metal grade hydrogen peroxide in a heating bath at 130 °C, and further dilution with doubly deionized water. Scandium was used to quantify Ca^{2+} by the external calibration method with an Agilent 8800 ICP-MS as previously described[17].

Linking of DTPA to PEI-coated conidia. To coat Δ*pksP* conidia with PEI, the conidia were added to the polymer solution (1 mg ml^{-1}, pH 5.5). The PEI solution was prepared by dissolving a known amount of the polymer in water and then adjusting its pH to 5.5 with a HCl solution. The mixture was left under stirring during at least 2 h, at room temperature. After washing the conidia twice with ultra-pure water using Vivaspin 300 kD Filter Units (Fisher Scientific), it was performed the covalent linking of DTPA to PEI. First, DTPA was activated using a mixture of EDC:NHS (50 mM:200 mM)[57] dissolved in 0.1 M MES buffer (pH 4.7) for 15 min at room temperature. Afterwards, PEI-coated conidia were incubated overnight at 4 °C with an extra amount of the activated DTPA. After this period of time, conidia were washed as described before.

Zeta-potential measurements. Zeta-potential values were obtained by laser Doppler electrophoresis. The measurements were performed in disposable folded capillary cells, at 25.0 ± 0.1 °C, in a Zetasizer Nano ZS equipment (Malvern Instruments). The electrostatic interaction of the polymer to the conidia was performed to pH 5.5, since PEI at this pH value has a strong positive charge (+49.0 + 1.3 mV) and non-modified Δ*pksP* present a negative charge at the same pH, −16.7 + 1.2 mV. The PEI coating as well as the binding of DTPA to PEI was confirmed by zeta-potential measurements (Supplementary Table 2). As can be observed from Supplementary Table 2, the Δ*pksP* and WT conidia present a negative charge (as already demonstrated in ref. [58]), which change to positive with PEI adsorption. This change in the surface electric charge of the conidia represents a good parameter to evaluate the polymer electrostatic interaction with conidia. Indeed, as PEI presents a positive charge, it is expected that its adsorption to the conidia surface will result in a positive charge.

The linking of DTPA at the surface of conidia was performed using PEI amino groups and an ethyl(dimethylaminopropyl) carbodiimide (EDC)/N-hydroxysuccinimide (NHS) solution. The covalent coupling of this metal chelating agent was verified by a change in the charge of the PEI-coated conidia, since this ethylenediaminetatraacetic acid (EDTA) like ligand have a negative charge at pH 7. The Ca^{2+} chelating properties of DTPA-PEI-coated Δ*pksP* conidia were validated via ion chromatography analysis.

Human studies. A total of 310 haematologic patients undergoing allogeneic haematopoietic stem-cell transplantation at the Hospital of Santa Maria, Lisbon and Instituto Português de Oncologia (IPO), Porto, between 2009 and 2014 were enrolled in the study[19], including 66 cases of probable/proven aspergillosis and 244 uninfected controls. The cases of invasive aspergillosis were identified and classified as 'probable' or 'proven' according to the revised standard criteria from the European Organization for Research and Treatment of Cancer/Mycology Study Group (EORTC/MSG)[59]. Study approval for the genetic association study was obtained from the Ethics Subcommittee for Life and Health Sciences of the University of Minho, Portugal (125/014), the Ethics Committee for Health of the Instituto Português de Oncologia - Porto, Portugal (26/015), the Ethics Committee of the Lisbon Academic Medical Center, Portugal (632/014), and the National Commission for the Protection of Data, Portugal (1950/015). Approval for the collection of blood for functional studies on monocytes was obtained from the Ethics Subcommittee for Life and Health Sciences of the University of Minho, Portugal (SECVS-014/2015) and the Ethics Committee of the University Hospital of Heraklion, Crete, Greece (5159/2014). Approval for BAL collection was obtained from the Ethics Subcommittee for Life and Health Sciences of the University of Minho, Portugal (126/014), and the Ethics Committee of the University Hospitals of Leuven, Belgium. All individuals provided written informed consent in accordance with the Declaration of Helsinki.

Genomic DNA was isolated from whole blood using the QIAcube automated system (Qiagen). Genotyping of the rs12885713 SNP in the *CALM1* gene was performed using KASPar assays (LGC Genomics) in an Applied Biosystems 7500 Fast PCR system (Thermo Fisher).

Statistical analysis. The data were expressed as means ± s.e.m. Statistical significance of differences were determined by two-tailed Student's *t*-test and one-way ANOVA with the indicated post hoc test for multiple comparisons. ($P<0.05$ was considered statistically significant). Analysis was done in GraphPad Prism software. The probability of invasive aspergillosis resulting from *CALM1* rs12885713 genotypes was analysed using the cumulative incidence method and compared using Gray's test[19,60]. Cumulative incidences were computed with the *cmprsk* package for R version 2.10.1, with censoring of data at the date of last follow-up visit and defining relapse and death as competing events[60]. A period of 24 months after transplant was chosen to include all cases of fungal infection.

Reporting Summary. Further information on experimental design is available in the Nature Research Reporting Summary linked to this article.

Data availability. All the data that support the findings of this study are available from the corresponding author upon reasonable request.

Received: 25 August 2017; Accepted: 23 April 2018;
Published online: 30 May 2018

References

1. Sanjuan, M. A. et al. Toll-like receptor signalling in macrophages links the autophagy pathway to phagocytosis. *Nature* **450**, 1253–1257 (2007).
2. Martinez, J. et al. Molecular characterization of LC3-associated phagocytosis reveals distinct roles for Rubicon, NOX2 and autophagy proteins. *Nat. Cell. Biol.* **17**, 893–906 (2015).
3. Green, D. R., Oguin, T. H. & Martinez, J. The clearance of dying cells: table for two. *Cell Death Differ.* **23**, 915–926 (2016).
4. Martinez, J. et al. Noncanonical autophagy inhibits the autoinflammatory, lupus-like response to dying cells. *Nature* **533**, 115–119 (2016).
5. Chu, H. et al. Gene-microbiota interactions contribute to the pathogenesis of inflammatory bowel disease. *Science* **352**, 1116–1120 (2016).
6. Kyrmizi, I. et al. Corticosteroids block autophagy protein recruitment in *Aspergillus fumigatus* phagosomes via targeting dectin-1/Syk kinase signalling. *J. Immunol.* **191**, 1287–1299 (2013).
7. Akoumianaki, T. et al. Aspergillus cell wall melanin blocks LC3-associated phagocytosis to promote pathogenicity. *Cell Host Microbe* **19**, 79–90 (2016).
8. de Luca, A. et al. IL-1 receptor blockade restores autophagy and reduces inflammation in chronic granulomatous disease in mice and in humans. *Proc. Natl Acad. Sci. USA* **111**, 3526–3531 (2014).
9. Oikonomou, V. et al. Noncanonical fungal autophagy inhibits inflammation in response to IFN-gamma via DAPK1. *Cell Host Microbe* **20**, 744–757 (2016).
10. Nunes, P. & Demaurex, N. The role of calcium signalling in phagocytosis. *J. Leukoc. Biol.* **88**, 57–68 (2010).
11. Hoyer-Hansen, M. et al. Control of macroautophagy by calcium, calmodulin-dependent kinase kinase-beta, and Bcl-2. *Mol. Cell* **25**, 193–205 (2007).
12. Lennartz, M. R., Lefkowith, J. B., Bromley, F. A. & Brown, E. J. Immunoglobulin G-mediated phagocytosis activates a calcium-independent, phosphatidylethanolamine-specific phospholipase. *J. Leukoc. Biol.* **54**, 389–398 (1993).
13. Ganley, I. G., Wong, P. M., Gammoh, N. & Jiang, X. Distinct autophagosomal-lysosomal fusion mechanism revealed by thapsigargin-induced autophagy arrest. *Mol. Cell* **42**, 731–743 (2011).
14. Malik, Z. A., Denning, G. M. & Kusner, D. J. Inhibition of Ca^{2+} signalling by Mycobacterium tuberculosis is associated with reduced phagosome-lysosome fusion and increased survival within human macrophages. *J. Exp. Med.* **191**, 287–302 (2000).
15. Vergne, I., Chua, J. & Deretic, V. Tuberculosis toxin blocking phagosome maturation inhibits a novel Ca^{2+}/calmodulin-PI3K hVPS34 cascade. *J. Exp. Med.* **198**, 653–659 (2003).
16. Zheng, L., Nibbering, P. H. & van Furth, R. Cytosolic free calcium is essential for immunoglobulin G-stimulated intracellular killing of *Staphylococcus aureus* by human monocytes. *Infect. Immun.* **60**, 3092–3097 (1992).
17. Subramanian Vignesh, K., Landero Figueroa, J. A., Porollo, A., Caruso, J. A. & Deepe, G. S. Jr. Granulocyte macrophage-colony stimulating factor induced

Zn sequestration enhances macrophage superoxide and limits intracellular pathogen survival. *Immunity* **39**, 697–710 (2013).
18. Mototani, H. et al. A functional single nucleotide polymorphism in the core promoter region of CALM1 is associated with hip osteoarthritis in Japanese. *Hum. Mol. Genet.* **14**, 1009–1017 (2005).
19. Cunha, C. et al. IL-10 overexpression predisposes to invasive aspergillosis by suppressing antifungal immunity. *J. Allergy Clin. Immunol.* S0091-6749(17)30515-8 [pii]10.1016/j.jaci.2017.0 (2017).
20. Matte, C. et al. Leishmania major promastigotes evade LC3-associated phagocytosis through the action of GP63. *PLoS Pathog.* **12**, e1005690 (2016).
21. Boonhok, R. et al. LAP-like process as an immune mechanism downstream of IFN-gamma in control of the human malaria *Plasmodium vivax* liver stage. *Proc. Natl Acad. Sci. USA* **113**, E3519–3528 (2016).
22. Li, X. et al. Lyn delivers bacteria to lysosomes for eradication through TLR2-initiated autophagy related phagocytosis. *PLoS Pathog.* **12**, e1005363 (2016).
23. Malik, Z. A., Iyer, S. S. & Kusner, D. J. Mycobacterium tuberculosis phagosomes exhibit altered calmodulin-dependent signal transduction: contribution to inhibition of phagosome-lysosome fusion and intracellular survival in human macrophages. *J. Immunol.* **166**, 3392–3401 (2001).
24. Sawyer, D. W., Sullivan, J. A. & Mandell, G. L. Intracellular free calcium localization in neutrophils during phagocytosis. *Science* **230**, 663–666 (1985).
25. Stendahl, O. et al. Redistribution of intracellular Ca^{2+} stores during phagocytosis in human neutrophils. *Science* **265**, 1439–1441 (1994).
26. Steinckwich, N., Schenten, V., Melchior, C., Brechard, S. & Tschirhart, E. J. An essential role of STIM1, Orai1, and S100A8-A9 proteins for Ca^{2+} signalling and FcgammaR-mediated phagosomal oxidative activity. *J. Immunol.* **186**, 2182–2191 (2011).
27. Worth, R. G., Kim, M. K., Kindzelskii, A. L., Petty, H. R. & Schreiber, A. D. Signal sequence within Fc gamma RIIA controls calcium wave propagation patterns: apparent role in phagolysosome fusion. *Proc. Natl Acad. Sci. USA* **100**, 4533–4538 (2003).
28. Nunes, P. et al. STIM1 juxtaposes ER to phagosomes, generating Ca^{2+} hotspots that boost phagocytosis. *Curr. Biol.* **22**, 1990–1997 (2012).
29. Guido, D., Demaurex, N. & Nunes, P. Junctate boosts phagocytosis by recruiting endoplasmic reticulum Ca^{2+} stores near phagosomes. *J. Cell Sci.* **128**, 4074–4082 (2015).
30. Campbell-Valois, F. X. et al. Quantitative proteomics reveals that only a subset of the endoplasmic reticulum contributes to the phagosome. *Mol. Cell Proteom.* **11**, 016378 (2012).
31. Kelly, E. K., Wang, L. & Ivashkiv, L. B. Calcium-activated pathways and oxidative burst mediate zymosan-induced signalling and IL-10 production in human macrophages. *J. Immunol.* **184**, 5545–5552 (2010).
32. Cathcart, M. K. Regulation of superoxide anion production by NADPH oxidase in monocytes/macrophages: contributions to atherosclerosis. *Arterioscler. Thromb. Vasc. Biol.* **24**, 23–28 (2004).
33. Yang, C. S. et al. Autophagy protein Rubicon mediates phagocytic NADPH oxidase activation in response to microbial infection or TLR stimulation. *Cell Host Microbe* **11**, 264–276 (2012).
34. Arnaudeau, S., Kelley, W. L., Walsh, J. V. Jr. & Demaurex, N. Mitochondria recycle Ca^{2+} to the endoplasmic reticulum and prevent the depletion of neighboring endoplasmic reticulum regions. *J. Biol. Chem.* **276**, 29430–29439 (2001).
35. Riazanski, V. et al. TRPC6 channel translocation into phagosomal membrane augments phagosomal function. *Proc. Natl Acad. Sci. USA* **112**, E6486–6495 (2015).
36. Vaeth, M. et al. Ca^{2+} signalling but not store-operated Ca^{2+} entry is required for the function of macrophages and dendritic cells. *J. Immunol.* **195**, 1202–1217 (2015).
37. Westphalen, K. et al. Sessile alveolar macrophages communicate with alveolar epithelium to modulate immunity. *Nature* **506**, 503–506 (2014).
38. Zelante, T. et al. $CD103^{+}$ dendritic cells control Th17 cell function in the lung. *Cell Rep.* **12**, 1789–1801 (2015).
39. Liu, Y. & Simon, J. D. Metal-ion interactions and the structural organization of Sepia eumelanin. *Pigment Cell Res.* **18**, 42–48 (2005).
40. d'Ischia, M. et al. Melanins and melanogenesis: from pigment cells to human health and technological applications. *Pigment Cell Melanoma Res.* **28**, 520–544 (2015).
41. Hong, L. & Simon, J. D. Current understanding of the binding sites, capacity, affinity, and biological significance of metals in melanin. *J. Phys. Chem. B* **111**, 7938–7947 (2007).
42. Drager, U. C. Calcium binding in pigmented and albino eyes. *Proc. Natl Acad. Sci. USA* **82**, 6716–6720 (1985).
43. Bush, W. D. & Simon, J. D. Quantification of Ca^{2+} binding to melanin supports the hypothesis that melanosomes serve a functional role in regulating calcium homeostasis. *Pigment Cell Res.* **20**, 134–139 (2007).
44. Hoogduijn, M. J. et al. Melanin has a role in Ca^{2+} homeostasis in human melanocytes. *Pigment Cell Res.* **16**, 127–132 (2003).
45. Biesemeier, A., Schraermeyer, U. & Eibl, O. Quantitative chemical analysis of ocular melanosomes in stained and non-stained tissues. *Micron* **42**, 461–470 (2011).
46. Meyer zum Gottesberge, A. M. Physiology and pathophysiology of inner ear melanin. *Pigment Cell Res.* **1**, 238–249 (1988).
47. Zecca, L. et al. The neuromelanin of human substantia nigra and its interaction with metals. *J. Neural Transm. (Vienna)* **109**, 663–672 (2002).
48. Malik, Z. A. et al. Cutting edge: *Mycobacterium tuberculosis* blocks Ca^{2+} signalling and phagosome maturation in human macrophages via specific inhibition of sphingosine kinase. *J. Immunol.* **170**, 2811–2815 (2003).
49. Vergne, I., Chua, J. & Deretic, V. *Mycobacterium tuberculosis* phagosome maturation arrest: selective targeting of PI3P-dependent membrane trafficking. *Traffic* **4**, 600–606 (2003).
50. Lin, Y. P., Raman, R., Sharma, Y. & Chang, Y. F. Calcium binds to leptospiral immunoglobulin-like protein, LigB, and modulates fibronectin binding. *J. Biol. Chem.* **283**, 25140–25149 (2008).
51. Sebghati, T. S., Engle, J. T. & Goldman, W. E. Intracellular parasitism by *Histoplasma capsulatum*: fungal virulence and calcium dependence. *Science* **290**, 1368–1372 (2000).
52. Takematsu, H. & Seiji, M. Effect of macrophages on elimination of dermal melanin from the dermis. *Arch. Dermatol. Res* **276**, 96–98 (1984).
53. Xiang, W., Song, X., Peng, J., Xu, A. & Bi, Z. Real-time in vivo confocal laser scanning microscopy of melanin-containing cells: a promising diagnostic intervention. *Microsc. Res. Tech.* **78**, 1121–1127 (2015).
54. Nakamura, S. et al. Melanin-laden macrophages in cerebrospinal fluid in Vogt-Koyanagi-Harada syndrome. *Arch. Ophthalmol.* **114**, 1184–1188 (1996).
55. Polak, M. E. et al. Mechanisms of local immunosuppression in cutaneous melanoma. *Br. J. Cancer* **96**, 1879–1887 (2007).
56. Tsai, H. F., Chang, Y. C., Washburn, R. G., Wheeler, M. H. & Kwon-Chung, K. J. The developmentally regulated alb1 gene of *Aspergillus fumigatus*: its role in modulation of conidial morphology and virulence. *J. Bacteriol.* **180**, 3031–3038 (1998).
57. Oliveira, C., Costa-Pinto, A. R., Reis, R. L., Martins, A. & Neves, N. M. Biofunctional nanofibrous substrate comprising immobilized antibodies and selective binding of autologous growth factors. *Biomacromolecules* **15**, 2196–2205 (2014).
58. Wasylnka, J. A. & Moore, M. M. Adhesion of *Aspergillus* species to extracellular matrix proteins: evidence for involvement of negatively chargeddcarbohydrates on the conidial sdrface. *Infect. Immun.* **68**, 3377–3384 (2000).
59. De Pauw, B. et al. Revised definitions of invasive fungal disease from the European Organization for Research and Treatment of Cancer/Invasive Fungal Infections Cooperative Group and the National Institute of Allergy and Infectious Diseases Mycoses Study Group (EORTC/MSG) Consensus Group. *Clin. Infect. Dis.* **46**, 1813–1821 (2008).
60. Scrucca, L., Santucci, A. & Aversa, F. Competing risk analysis using R: an easy guide for clinicians. *Bone Marrow Transplant.* **40**, 381–387 (2007).

Acknowledgements

The authors would like to thank N. Tavernarakis for helpful suggestions and G. Garinis and A. Eliopoulos for providing antibodies and reagents. The authors are grateful to G. Chalepakis, E. Papadogiorgaki and other members of the electron microscopy facility at UOC.

I.K.'s work is supported by the Onassis Foundation under the 'Special Grant and Support Program for Scholars' Association Members' (Grant no. R ZM 003-1/2016-2017); G.C. was supported by grants from the Greek State Scholarship Foundation (I.K.Y.), the Hellenic General Secretariat for Research and Technology-Excellence program (ARISTEIA) and a Research Grant from Institut Mérieux; J.P.L. was supported by European Community's Seventh Framework Programme (FP7/2007-2013) under grant agreement 260338 ALLFUN and ANR-10-BLAN-1309 HYDROPHOBIN, and the Association Vaincre La Mucoviscidose (RF20140501052/1/1/141); H.F. and N.M.N. were supported by the project FROnTHERA (NORTE-01-0145-FEDER-000023), supported by Northern Portugal Regional Operational Programme (NORTE 2020), under the Portugal 2020 Partnership Agreement, through the European Regional Development Fund (ERDF), and by Fundação para a Ciência e Tecnologia (FCT) project SPARTAN (PTDC/CTM-BIO/4388/2014), funded through the PIDDAC Program. A.C. and C.C. were supported by NORTE 2020, under the Portugal 2020 Partnership Agreement, through the ERDF (NORTE-01-0145-FEDER-000013), and by FCT (IF/00735/2014 and SFRH/BPD/96176/2013). G.S.D. and J.L.F. were supported by NIH grant AI-106269. K.J.K-C is supported by the Division of Intramural Research (DIR), NIAID, NIH.

Author contributions

I.K. designed, performed and analysed most of the experiments in this study, established protocols for Ca^{2+} imaging and phagosome processing and participated in the writing

of the manuscript. A.C. and C.C. performed experiments on analysis of CaLM1 SNPs in clinical samples. J.F.L. and A.C.Jr. provided patient samples and clinical information. L.F.J.A. performed ICP-MS measurements of Ca^{2+} content of phagosomes; P.Z. and N.P. performed Ion Chromatography Analysis of Ca^{2+} binding affinity of *A. fumigatus* conidia; T.A., G.S., D.P.K., G.S.D. Jr and A.B. analysed data and provided suggestions throughout the study. K.S. performed electron microscopy studies. J.E. and K.J.K. provided reagents and analysed data. H.F. and N.M.N. developed, produced and characterized the DTPA-PEI-coated conidia; A.B. generated *A. fumigatus* purified melanin; I.V and J.P.L. generated *A. fumigatus* mutants and provided reagents, analysed data and provided discussions and suggestions throughout the study. G.C. conceived and supervised the study, performed experiments, was involved in the design and evaluation of all experiments, and wrote the manuscript along with comments from co-authors.

Competing interests

The authors declare no competing interests.

Additional information

Supplementary information is available for this paper at https://doi.org/10.1038/s41564-018-0167-x.

Reprints and permissions information is available at www.nature.com/reprints.

Correspondence and requests for materials should be addressed to G.C.

Publisher's note: Springer Nature remains neutral with regard to jurisdictional claims in published maps and institutional affiliations.

nature research

Corresponding author(s): Georgios Chamilos

Reporting Summary

Nature Research wishes to improve the reproducibility of the work that we publish. This form provides structure for consistency and transparency in reporting. For further information on Nature Research policies, see Authors & Referees and the Editorial Policy Checklist.

Statistical parameters

When statistical analyses are reported, confirm that the following items are present in the relevant location (e.g. figure legend, table legend, main text, or Methods section).

n/a	Confirmed	
☐	☒	The exact sample size (*n*) for each experimental group/condition, given as a discrete number and unit of measurement
☐	☒	An indication of whether measurements were taken from distinct samples or whether the same sample was measured repeatedly
☐	☒	The statistical test(s) used AND whether they are one- or two-sided *Only common tests should be described solely by name; describe more complex techniques in the Methods section.*
☐	☒	A description of all covariates tested
☐	☒	A description of any assumptions or corrections, such as tests of normality and adjustment for multiple comparisons
☐	☒	A full description of the statistics including central tendency (e.g. means) or other basic estimates (e.g. regression coefficient) AND variation (e.g. standard deviation) or associated estimates of uncertainty (e.g. confidence intervals)
☐	☒	For null hypothesis testing, the test statistic (e.g. *F*, *t*, *r*) with confidence intervals, effect sizes, degrees of freedom and *P* value noted *Give P values as exact values whenever suitable.*
☐	☒	For Bayesian analysis, information on the choice of priors and Markov chain Monte Carlo settings
☐	☒	For hierarchical and complex designs, identification of the appropriate level for tests and full reporting of outcomes
☐	☒	Estimates of effect sizes (e.g. Cohen's *d*, Pearson's *r*), indicating how they were calculated
☐	☒	Clearly defined error bars *State explicitly what error bars represent (e.g. SD, SE, CI)*

Our web collection on statistics for biologists may be useful.

Software and code

Policy information about availability of computer code

Data collection	Collection of images from confocal imaging was done by the use of LCS Lite Software, Leica
Data analysis	Analysis was done in GraphPad Prism software version 7.0.0, FlowJo R, Version 2.10.1 and Adobe Photoshop CS2

For manuscripts utilizing custom algorithms or software that are central to the research but not yet described in published literature, software must be made available to editors/reviewers upon request. We strongly encourage code deposition in a community repository (e.g. GitHub). See the Nature Research guidelines for submitting code & software for further information.

Data

Policy information about availability of data

All manuscripts must include a data availability statement. This statement should provide the following information, where applicable:

- Accession codes, unique identifiers, or web links for publicly available datasets
- A list of figures that have associated raw data
- A description of any restrictions on data availability

All unique material used in the study are readily available from the authors. Detailed information of commercially available material used in this study is provided in the methods section

Field-specific reporting

Please select the best fit for your research. If you are not sure, read the appropriate sections before making your selection.

☒ Life sciences ☐ Behavioural & social sciences

For a reference copy of the document with all sections, see nature.com/authors/policies/ReportingSummary-flat.pdf

Life sciences

Study design

All studies must disclose on these points even when the disclosure is negative.

Sample size	No statistical methods were used to predetermine sample size. Each of the experiments was repeated at least three different times for statistical comparisons
Data exclusions	No data were excluded from the analysis of all of the experiments.
Replication	All attempts at replication were successful in all experiments. All experiments were repeated at least once (i.e. at least 2 biologic replicates), and usually more often (typically in triplicate), as detailed for individual experiments in the paper (usually provided as an "n" value).
Randomization	Randomization is not relevant to our study, which included analysis of cellular assays and human samples that have been previously collected. All of the experiments were performed with primary immune cells (monocytes, macrophages). All cellular biology experiments always included a positive and negative control for meaningful comparisons with the experimental treatment groups.
Blinding	Evaluation of all experiments on phagosome biogenesis studies, EM analysis, and Ca2+ binding measurements was performed in a blinded fashion. A distinct number was allocated to each experimental condition. Acquisition and analysis of the samples by another investigator, when possible (e.g., FACS analysis, Ca2+ binding studies). Confocal imaging and scoring of phagosomes was performed by the same investigator in a blinded fashion. Blinding was not possible for live imaging studies because the discrimination of melanin plus and minus Aspergillus strains used for these studies is evident macroscopically Note

Materials & experimental systems

Policy information about availability of materials

n/a	Involved in the study
☐	☒ Unique materials
☐	☒ Antibodies
☒	☐ Eukaryotic cell lines
☐	☒ Research animals
☐	☒ Human research participants

Unique materials

Obtaining unique materials	All unique material used in the study are readily available from the authors. Detailed information of commercially available material used in this study is provided in the methods section

Antibodies

Antibodies used	The following antibodies were used in the study: a-Calmodulin (MA3-917, ThermoFisher Scientific; dilution 1:50), validated by the company for immunofluorescence (IF) studies. Also avaliable citations (e.g., J Cell Sci. 1993 Apr;104 (Pt 4):1119-27). In addition, validated in the present work by western blot and the effect of Ca2+ and CaM antagonist a-Calmodulin (NBP1-61548, Novus; dilution 1;100). Validated in the present work by western blot and the effect of Ca2+ and CaM antagonist. Validated by the company for WB analysis and IF studies a-LC3B (clone 5F10, Nanotools; dilution 1:20), extensively validated in published studies of our group (e.g., ref 6, 7) a-Vps34 (4263, Cell Signaling; dilution 1:20), Validated in previous studies on LAP (ref 2) a-PI(3)P (Z-P003, Echelon; dilution 1;100), Validated in previous studies on LAP (ref 2) a-p22 phox (sc-20781, Santa Cruz; dilution 1:100), validated in previous studies of our group (e.g. ref 7) a-p47 phox (610354 BD; dilution 1:100), (validate in previous studies of the group (e.g., ref 7) rabbit polycolocal anti-GFP (Minotech Biotechnology, Heraklion, Greece; dilution 1:500) (validated in previous published work (e.g. Palikaras et al., Nature. 2015 May 28;521(7553):525-8) a-Rubicon (ab156052, Abcam; dilution 1:50), validated by the company and previous studies on LAP (ref. 9) a-p40phox (clone D8, sc-48388, Santa Cruz; 1:100), validated by company and Dr Jamel-El Benna lab

a-ATG7 (ab133528, Abcam; dilution 1:50), validated by the Company and previous studies (ref. 9)
a-VATPase (ATP6V1B2; 73404, Abcam; dilution 1:100), validated by the company and experiments in our lab.
Antibody dilutions are also provided in the Methods section.

Validation

Validation statements for all antibodies, including images of Western blots in which human cell extracts containing the relevant protein are probed with the antibodies, are provided on the manufacturer website. Data provided in the manuscript also confirmed specific reactivity with the relevant protein. Additional references on antibody validation are provided.

Research animals

Policy information about studies involving animals; ARRIVE guidelines recommended for reporting animal research

Animals/animal-derived materials

C57BL/6 mice obtained from the IMBB Institute (Crete), and GFP-LC3 mice (obtained from RIKEN BioResource Center) were maintained in grouped cages in a High-Efficiency Particulate Air–filtered environmentally controlled virus-free facility (24°C, 12/12 h light/dark cycle), and fed by standard chow diet and water ad libitum. All experiments were approved by the local ethics committee of the University of Crete Medical School, Greece in line with the corresponding national and European Union legislation. BMDMs were generated by culturing BM cells obtained from 8 weeks old female mice in DMEM, supplemented with L929 cell-conditioned medium (30%). The resulting cultures consisted of macrophages (>95% purity), as determined by staining for F4/80 and flow cytometry.
Policy

Human research participants

Policy information about studies involving human research participants

Population characteristics

A total of 310 hematologic patients undergoing allogeneic hematopoietic stem cell transplantation at the Hospital of Santa Maria, Lisbon and Instituto Português de Oncologia (IPO), Porto, between 2009 and 2014 were enrolled in the study. Detailed clinical characteristics of these patients have been published in a previous study (ref. 19; Cunha, C. et al. IL-10 overexpression predisposes to invasive aspergillosis by suppressing antifungal immunity. J Allergy Clin Immunol, (2017). The cases of invasive aspergillosis were identified and classified as “probable” or “proven” according to the revised standard criteria from the European Organization for Research and Treatment of Cancer/Mycology Study Group (EORTC/MSG) 56.
Study approval for the genetic association study was obtained from the Ethics Subcommittee for Life and Health Sciences of the University of Minho, Portugal (125/014), the Ethics Committee for Health of the Instituto Português de Oncologia - Porto, Portugal (26/015), the Ethics Committee of the Lisbon Academic Medical Center, Portugal (632/014), and the National Commission for the Protection of Data, Portugal (1950/015). Approval for the collection of blood for functional studies on monocytes was obtained from the Ethics Subcommittee for Life and Health Sciences of the University of Minho, Portugal (SECVS-014/2015) and the Ethics Committee of the University Hospital of Heraklion, Crete, Greece (5159/2014). Approval for BAL collection was obtained from the Ethics Subcommittee for Life and Health Sciences of the University of Minho, Portugal (126/014), and the Ethics Committee of the University Hospitals of Leuven, Belgium. All individuals provided written informed consent in accordance with the Declaration of Helsinki.

Method-specific reporting

n/a	Involved in the study
☒	☐ ChIP-seq
☐	☒ Flow cytometry
☒	☐ Magnetic resonance imaging

Flow Cytometry

Plots

Confirm that:

☒ The axis labels state the marker and fluorochrome used (e.g. CD4-FITC).

☒ The axis scales are clearly visible. Include numbers along axes only for bottom left plot of group (a 'group' is an analysis of identical markers).

☒ All plots are contour plots with outliers or pseudocolor plots.

☒ A numerical value for number of cells or percentage (with statistics) is provided.

Methodology

Sample preparation

For ROS production, purified human primary human CD14+ monocytes (2 x 10^5/condition) were placed in 96 well round bottom plates, incubated at 37 C for 30 min and accordingly stimulated for 1h with A. fumigatus conidia of the indicated strain at a MOI 10:1, in the presence of DCFH-DA added to a final concentration of 10 uM during the last 30 min. After 30 min of exposure, the content of the wells was transfered to vials and the fluorescence of the cells from each well measured by flow cytometry.

For flow cytometry of phagosomes (phago-FACS), GFP-LC3 bone marrow derived macrophages (BMDMs) were stimulated with control magnetic beads or EDTA-magnetic beads at a ratio of 20:1 (bead: BMDM), phagosomes were isolated by magnetic separation, stained with an anti-GFP antibody, extensively washed with FACS buffer X 4 and the amount of GFP-LC3+ phagosomes was determined by FACS analysis.

Instrument	Cells were acquired on a FACSCalibur (BD Biosciences)
Software	All data were analyzed using FlowJo software (Tree Star)
Cell population abundance	he purity of human monocytes was determined by CD14+ staining following magnetic isolation and was typically > 95%
Gating strategy	For FACS analysis of ROS production, DCFH-DA florescence of unstimulated monocytes served as control for ROS production following stimulation with A. fumigatus conidia. For phago-FACS analysis, control magnetic beads stained with anti-GFP antibody served as an isotype control for GFP-LC3+ magentic-bead containing phagosomes The gating strategy for phago FACS analysis is shown in Figure 3

☐ Tick this box to confirm that a figure exemplifying the gating strategy is provided in the Supplementary Information.